Inorganic Chemistry

pubs.acs.org/IC
Article

Donor and Geometry Optimization: Fresh Perspectives for the Design of Polyoxometalate Charge Transfer Chromophores

Bethany R. Hood, Yovan de Coene, Claire F. Jones, Noah Deveaux, Jack M. Barber, Charlotte G. Marshall, Chloe A. Jordan, Nathan R. Halcovitch, Benoît Champagne,* Koen Clays,* and John Fielden*

Cite This: *Inorg. Chem.* 2025, 64, 8408−8420

ABSTRACT: Three linear, dipolar arylimido-polyoxometalate (POM) and one 2-dimensional *bis*-functionalized arylimido-polyoxometalate charge transfer chromophore, with diphenylacetylene bridges, have been synthesized and studied by spectroelectrochemistry, hyper-Rayleigh scattering (HRS), and DFT/TD-DFT calculations. The linear systems show that with julolidinyl (Jd) and $-NTol_2$ donor groups, the alkyne bridge yields high second-order nonlinear optical (NLO) coefficients β (Jd, $\beta_{0,zzz} = 318 \times 10^{-30}$ esu; $-NTol_2$, $\beta_{0,zzz} = 222 \times 10^{-30}$ esu), indeed the Jd compound gives the highest NLO activity of any organoimido-POM to date with minimal decrease in transparency. The *bis*-functionalized 2D (C_{2v}) POM derivative showed increased activity over its monofunctionalized analogue with no decrease in transparency, although the NLO response was only minimally two dimensional. Spectroelectrochemistry and TD-DFT calculations showed switchable linear optical responses for the monofunctionalized derivatives due to the weakened charge transfer character of the electronic transitions in the reduced state, while TD-DFT also indicated potential for switched NLO responses. These have been demonstrated by electrochemistry-HRS for the Jd compound, but cyclability is limited by relatively poor stability in the reduced state. IR and CV studies for these sterically protected arylimido polyoxometalates indicate that decomposition proceeds via a breakdown of the $\{Mo_6\}$ cluster in the reduced state, rather than simple solvolysis of the Mo≡N bond.

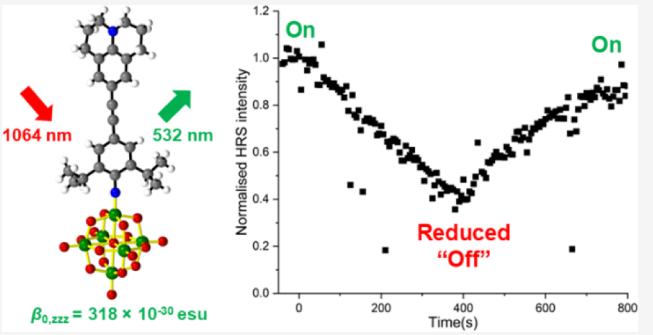

INTRODUCTION

Polyoxometalates (POMs) are a vast family of anionic cluster compounds consisting primarily of transition metal ions (typically Mo and W) in their highest oxidation state and both bridging and terminal oxo ligands.[1] Their extensive range of sizes—all the way from subnanometer $\{M_5\}$ and $\{M_6\}$ clusters to giant, multinanometer architectures such as $\{Mo_{368}\}$—shapes,[2] rich redox chemistry, and ability to incorporate heteroatoms lead to a wide range of potential uses in areas including catalysis,[3] medicine,[4] and data storage.[5] Moreover, POMs can be derivatized with organic ligands,[6] further expanding and modulating their range of properties and applications. Here and in previous work, our focus is on arylimido Lindqvist POMs because conjugation between aryl unit and POM across the imido bond enables stronger electronic communication between the organic donor/π-system and POM core than typically seen in other functionalized POMs based on more electronically isolating W-O-X-Ar linkages (where X = main group elements, e.g., Si, P, As, and Sn). This is reflected in strongly shifted redox potentials, new electronic transitions, and *emergent* properties such as nonlinear optical (NLO) activity[7]—most of all, second-order effects (e.g., laser frequency doubling). These are essential to many technologies that rely on manipulation of laser light, and the fast responses obtained from molecular chromophores (including "POMophore" systems) could enable potential uses in telecommunications and optical/electro-optical computing.[8]

Two key challenges for molecular NLO materials are addressing nonlinearity/transparency trade-offs,[9] and making materials whose properties can be reversibly switched between two or more states.[10] The former is important because modifications that increase activity tend to increase visible and NIR light absorption, potentially affecting efficiency and stability of any device. The latter is relevant to the development of molecular optical and nonlinear optical transistors, memory devices, and sensors. POMophores[7] have shown promise in these areas, by enabling high NLO

Received: February 26, 2025
Revised: March 27, 2025
Accepted: April 2, 2025
Published: April 14, 2025

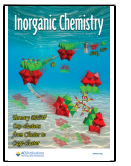

https://doi.org/10.1021/acs.inorgchem.5c00915
Inorg. Chem. 2025, 64, 8408−8420

coefficients β to be obtained from short, stable π-bridges that minimize visible-light absorption, and in one example showing highly cyclable electrochemically switched NLO responses,[11] without using metal donors (e.g., Ru^{II}) which tend to introduce low-energy visible absorptions.

In this work, we explore developing POM-based NLO chromophores and redox switches in terms of activity, transparency, and ease of synthesis. Stabilizing the arylimido Mo≡N bond enough to allow reversible multicycle redox switching depends on use of bulky groups (i.e., ^{i}Pr) in the 2,6 positions of the ring, and our previous work featured these on a single phenyl bridge linking the POM to an $-NMe_2$ donor.[11] Changes of donor (D) can give big increases in β and thus higher "on" state signal, but suitable ^{i}Pr-derivatized phenylaniline precursors are not readily accessible. Therefore, we investigate diphenylacetylene-bridged POM chromophores for redox-mediated NLO switching for the first time, investigating the effect of $-NMe_2$, $-NTol_2$, and julolidinyl (Jd) donors that can be attached to iodo-arylimido-POM precursors through well-established Sonogashira methods, and also test the effect of introducing a second donor group in a 2-dimensional (C_{2v}) D-A-D geometry (A = acceptor POM). The results reveal a new record POMophore response for the -Jd donor ($\beta_{0,zzz} = 320 \times 10^{-30}$ esu), showing for the first time that very strong alkylamino donors can exceed the performance of arylamino systems ($-NTol_2$ and $-NPh_2$), and indicate that D-A-D POMophores can increase response without sacrificing transparency. They also show the diphenylethyne-bridged systems can be redox switched but undergo a redox-induced decomposition of the POM core.

EXPERIMENTAL SECTION

Materials and Procedures. Anhydrous dimethyl sulfoxide (DMSO) was purchased from Sigma-Aldrich (SureSeal) and Acros Organics (AcroSeal) and used as supplied. All other reagents and solvents were obtained as ACS grade from Sigma-Aldrich, Alfa Aesar, Fisher Scientific, Fluorochem, Acros Organics, or Apollo Scientific and used as supplied. Deuterated solvents were obtained from Eurisotop, Cambridge Isotope Laboratories, or Acros Organics and used as supplied. Tetrabutylammonium hexamolybdate was synthesized according to previously reported methods.[12] 4-Iodo-2,6-diisopropylaniline (**P1**), iodo-arylimido polyoxometalates $[NBu_4]_2[Mo_6O_{18}NC_{12}H_{16}I]$ ($[NBu_4]_2$[**P2**]) and $[NBu_4]_2[Mo_6O_{17}(NC_{12}H_{16}I)_2]$ ($[NBu_4]_2$[**P3**]), and all other precursor compounds (**P4** to **P8**) were synthesized by using or adapting known methods, with full details and references given in the Supporting Information. Unless otherwise stated, reactions were performed under an atmosphere of dry argon using standard Schlenk techniques.

General Physical Measurements. FT-IR spectra were measured using a Bruker FT-IR XSA spectrometer. ^{1}H and ^{13}C NMR spectra were acquired using a Bruker Ascend 500 (500 MHz) spectrometer and all shifts are quoted with respect to TMS using the solvent signals as a secondary standard (s = singlet, d = doublet, t = triplet, q = quartet, quin = quintet, sex = sextet, *a*sex = apparent sextet, hept = heptet, m = multiplet). Some quaternary carbon signals were not observed for these compounds, similar to previously synthesized arylimido-polyoxometalates.[7] Elemental analyses and accurate mass spectrometry were outsourced to the University of Manchester and the John Innes Centre (Norwich), respectively. UV−vis spectra were obtained using an Agilent Cary 60 UV−vis spectrophotometer.

Preparation of $[NBu_4]_2[Mo_6O_{18}N_2C_{22}H_{26}]$ ($[NBu_4]_2$[1]). Compound **P2** (0.617 g, 0.374 mmol), 4-ethynyl-*N*,*N*-dimethylaniline (0.0652 g, 0.449 mmol), bis(triphenylphosphine) palladium(II) dichloride (7.4 mg, 0.011 mmol), copper iodide (3.4 mg, 0.018 mmol), and potassium carbonate (0.375 g, 2.7 mmol) were dissolved in dry acetonitrile (15 mL) before dry triethylamine (0.75 mL, 5.375 mmol) was added. The resulting mixture was stirred at room temperature for 30 min before the filtrate was evaporated to 2 mL and poured into diethyl ether (50 mL) resulting in a dark-red precipitate. This was collected by filtration, washed with diethyl ether, and then dried in vacuo to give $[NBu_4]_2$[**1**] as a dark-red solid (0.332 g, 0.201 mmol, 54%). ^{1}H NMR (500 MHz, CD_3CN): δ 7.37 (d, J = 9.0 Hz, 2H), 7.25 (s, 2H), 6.73 (d, J = 9.0 Hz, 2H), 3.83 (hept, J = 6.9 Hz, 2H), 3.13−3.06 (m, 16H), 2.98 ppm (s, 6H), 1.66−1.56 (m, 16H), 1.36 (*a*sex, J = 7.5 Hz, 16H), 1.31 (d, J = 6.8 Hz, 12H), 0.97 (t, J = 7.4 Hz, 24H). ^{13}C NMR (400 MHz, CD_3CN): δ 151.64, 149.83, 133.62, 125.71, 124.59, 112.85, 109.87, 94.12, 88.41, 68.25, 59.30, 40.32, 29.43, 24.32, 23.97, 20.31, 13.79. Anal. calcd % for $C_{54}H_{98}N_4O_{18}Mo_6$ ($[NBu_4]_2$[**1**]): C, 38.90 (38.90); H, 5.93 (5.89); N, 3.36 (3.35). HRMS (ESI, MeCN) m/z: 592.7750, calcd for $C_{22}H_{26}N_2Mo_6O_{18}^{2-}$ ($[\mathbf{1}]^{2-}$), 591.7767. FTIR (ATR) cm^{-1}: 2960 (m), 2932 (sh), 2872 (m), 2187 (m), 1606 (m), 1585 (m), 1585 (s), 1521 (m), 1445 (m), 1350 (w), 1227 (w), 1191 (m), 1169 (m), 1150 (m), 1063 (w), 974 (s), 943 (m), 882 (w), 855 (sh), 769 (w), 740 (sh). UV−vis (MeCN) λ, nm (ε, M^{-1} cm^{-1}): 203 (73.6×10^3), 293 (37.1×10^3), 424 (37.6×10^3).

Preparation of $[NBu_4]_2[Mo_6O_{18}N_2C_{34}H_{34}]$ ($[NBu_4]_2$[2]). Compound **P2** (1.433 g, 0.941 mmol), 4-ethylyphenyl-4,4′-ditolylamine (**P6**) (0.4163 g, 1.428 mmol), $(PPh_3)_2PdCl_2$ (12.6 mg, 0.018 mmol), copper iodide (8 mg, 0.042 mmol), and potassium carbonate (0.898 g, 6.50 mmol) were dissolved in dry acetonitrile (35 mL) before dry triethylamine (1.8 mL, 12.9 mmol) was added. The mixture was stirred for 80 min at room temperature before the filtrate was evaporated to 3 mL and poured into diethyl ether (200 mL). The resulting dark red precipitate was collected by filtration, washed with ethanol and diethyl ether, and then dried in vacuo to give compound $[NBu_4]_2$[**2**] as a dark-red solid (0.795 g, 0.438 mmol, 47%). ^{1}H NMR (500 MHz, CD_3CN): δ 7.33 (d, J = 8.8 Hz, 2H), 7.28 (s, 2H), 7.16 (d, J = 8.1 Hz, 4H), 7.00 (d, J = 8.4 Hz, 4H), 6.86 (d, J = 8.8 Hz, 2H), 3.83 (hept, J = 6.7 Hz, 2H), 3.15−3.06 (m, 16H), 2.31 (s, 6H), 1.66−1.56 (m, 16H), 1.38 (*a*sex, J = 8.0 Hz, 16H), 1.31 (d, J = 6.8 Hz, 12H), 0.97 (t, J = 7.4 Hz, 24H). ^{13}C NMR (126 MHz, CD_3CN): δ 149.80, 145.35, 134.99, 133.43, 131.11, 126.50, 126.00, 121.05, 59.28, 29.43, 24.31, 23.94, 20.84, 20.30, 13.78. Anal. calcd % for $C_{66}H_{106}N_4O_{18}Mo_6$ ($[NBu_4]_2$[**2**]): C, 43.57 (43.89); H, 5.87 (6.03); N, 3.08 (3.02). HRMS (ESI, MeCN) m/z: 666.8062, calcd for $C_{34}H_{34}N_2Mo_6O_{18}^{2-}$ ($[\mathbf{2}]^{2-}$), 666.8079. FTIR (ATR) cm^{-1}: 2959 (s), 2932 (m), 2872 (m), 2189 (w), 1600 (sh), 1585 (s), 1503 (vs), 1480 (s), 1380 (m), 1320 (s), 1294 (m), 1277 (m), 1151 (w), 1107 (w), 1067 (w), 1031 (w), 974 (s), 944 (vs), 880 (s), 774 (vs). UV−vis (MeCN) λ, nm (ε, M^{-1} cm^{-1}): 206 (90.4×10^3), 294 (33.1×10^3), 329 (19.0×10^3), 423 (39.4×10^3).

Preparation of $[NBu_4]_2[Mo_6O_{18}N_2C_{26}H_{30}]$ ($[NBu_4]_2$[3]). To a mixture of compound **P3** (0.618 g, 0.388 mmol), 4-ethynyljuloloidine (**P8**) (0.106 g, 0.537 mmol), bis(triphenylphosphine)palladium(II) chloride (0.009 g, 0.013 mmol), copper iodide (0.003 g, 0.027 mmol), and potassium carbonate (0.361 g, 2.61 mmol) in 15 mL of dry acetonitrile, dry triethylamine (0.8 mL, 5.74 mmol) was added. The resulting mixture was stirred at room temperature for 30 min before filtering, evaporating to 2 mL, and pouring into 50 mL of diethyl ether. The resulting red oil was collected by decanting the solution then washing with ethyl acetate and diethyl ether. Drying in vacuo yielded crude compound $[NBu_4]_2$[**3**] as a dark-red solid (0.372 g, 0.216 mmol, 56%). Further purification of 90 mg of the sample was achieved by crystallization by diffusion of diethyl ether into an acetone solution, to give pure $[NBu_4]_2$[**3**] (0.041 g, 0.024 mmol) in an overall 26% yield. ^{1}H NMR (500 MHz, $(CD_3)_2CO$): δ 7.18 (s, 2H), 6.88 (s, 2H), 3.98 (sept, J = 6.8 Hz, 2H), 3.47−3.44 (m, 16H), 3.21 (t, J = 5.7 Hz, 4H), 2.70 (t, J = 6.3, 4H), 1.92 (m, 4H), 1.86−1.80 (m, 16H), 1.45 (*a*sex, J = 6.8 Hz, 16H), 1.32 (d, J = 6.9 Hz, 12H), 0.98 (t, J = 7.3 Hz, 24H). ^{13}C NMR (126 MHz, $(CD_3)_2CO$): δ 131.09, 125.29, 121.85, 59.37, 50.42, 28.17, 24.54, 24.16, 22.44, 20.41, 15.61, 13.96. Anal. calcd % for $C_{58}H_{102}N_4O_{18}Mo_6$: C, 40.52 (40.86); H, 5.98 (5.95); N, 3.26 (3.24). HRMS (ESI, MeCN) m/z: 617.7923, calcd for $C_{26}H_{30}N_2Mo_6O_{18}^{2-}$ ($[\mathbf{3}]^{2-}$), 617.7933. FTIR (ATR) cm^{-1}:

https://doi.org/10.1021/acs.inorgchem.5c00915
Inorg. Chem. 2025, 64, 8408−8420

2960 (m), 2933 (sh), 2872 (m), 2187 (m), 1605 (sh), 1584 (m), 1511 (m), 1464 (m), 1380 (w), 1310 (m), 1249 (vw), 1208 (vw), 1185 (vw), 1145 (vw), 1170 (vw), 1052 (vw), 1030 (vw), 973 (m), 943 (s), 880 (m), 765 (s), 609 (w). UV−vis (MeCN) λ, nm (ε, M^{-1} cm^{-1}): 212 (65.3 × 10^3), 259 (30.3 × 10^3), 308 (30.0 × 10^3), 445 (37.8 × 10^3).

Preparation of $[NBu_4][Mo_6O_{17}(N_2C_{22}H_{16})_2]$ ($[NBu_4]_2$[4]). To compound **P8** (0.116 g, 0.060 mmol) were added 4-ethynyl-*N*,*N*-dimethylaniline (0.029 g, 0.20 mmol), bis(triphenylphosphine) palladium(II) dichloride (8.5 mg, 0.012 mmol), copper iodide (5.2 mg, 0.027 mmol), potassium carbonate (0.597 g, 4.31 mmol), 8 mL dry acetonitrile, and triethylamine (0.8 mL, 5.74 mmol). The resulting red solution was stirred for 40 min to give a brown solution which was filtered, evaporated to ∼1 mL, and then precipitated with 15 mL of diethyl ether. The resulting dark-red precipitate was collected by filtration, washed with ethyl acetate and diethyl ether, and then dried in vacuo to yield compound $[NBu_4]_2$[**4**] as a dark-red solid (0.079 g, 0.040 mmol, 67%). ^{1}H NMR (500 MHz, CD_3CN): δ 7.36 (d, J = 9.0 Hz, 4H), 7.23 (s, 4H), 6.73 (d, J = 9.0 Hz, 4H), 3.88 (hept, J = 6.8 Hz, 16H), 3.11−3.03 (m, 16H), 2.89 (s, 12H), 1.65−1.55 (m, 16H), 1.36 (*a*sex, J = 7.4 Hz, 16H), 1.30 (d, J = 6.8 Hz, 24H), 0.96 (t, J = 7.4 Hz, 24H). ^{13}C NMR (126 MHz, CD_3CN): δ 149.12, 133.60, 125.74, 112.92, 59.36, 47.72, 40.38, 29.35, 24.34, 24.12, 20.35, 13.82. Anal. calcd % for $C_{76}H_{124}N_6O_{17}Mo_6$: C, 46.35 (43.33); H, 6.35 (5.92); N, 4.27 (4.12). HRMS (ESI, MeCN): calcd for $C_{44}H_{52}N_4Mo_6O_{17}^{2-}$, 742.8852; found, 742.8844. FTIR (ATR) cm^{-1}: 2960 (m), 2932 (sh), 2871 (m), 2810 (sh), 2188 (m), 1731 (w), 1606 (m), 1585 (s), 1521 (m), 1460 (m), 1444 (m), 1350 (m), 1242 (w), 1191 (m), 1150 (w), 1062 (w), 1043 (w), 965 (m), 942 (vs), 880 (m), 760 (vs). UV−vis (MeCN) λ, nm (ε, M^{-1} cm^{-1}): 204 (108.7 × 10^3), 246 (48.1 × 10^3), 295 (50.6 × 10^3), 420 (56.7 × 10^3).

Electrochemistry. Cyclic voltammetry and bulk electrolysis experiments were carried out using an Autolab PGstat 30 or PGstat 302 potentiostat/galvanostat. Measurements were performed in a three compartment cell using a silver wire reference electrode, a glassy carbon working electrode, and a platinum wire counter electrode. Acetonitrile was freshly distilled (from CaH_2) and $[N(C_4H_9\text{-}n)_4]BF_4$[13] was used as the supporting electrolyte. Solutions containing ca. 0.8 mM analyte (0.1 M electrolyte) were degassed by purging with argon and blanketed with a continuous flow of argon throughout the experiments. $E_{1/2}$ values were calculated from $(E_{pa} + E_{pc})/2$ at a scan rate of 100 mV s^{-1} and referenced to Fc/Fc^+. For bulk electrolysis, reduction of the bulk sample was achieved by application of a potential of −0.7 V vs $Ag^{0/+}$ by a Pt gauze to the vigorously stirred solution for a total of 23 min. After this time, the current had plateaued at a current of near 0 A showing no further reduction was taking place.

Spectroelectrochemistry. All measurements were performed using a Spectroelectrochemistry Reading RT OTTLE cell,[14] with an Agilent Cary 60 UV−vis spectrophotometer and Autolab μ-III potentiostat. The analyte concentration was ca. 0.8 × 10^{-3} M in 0.3 M NBu_4BF_4 in dry acetonitrile. A reductive potential of between −0.8 and −0.5 V vs Ag was applied for between two and 5 min, varied to account for potential drift determined by a cyclic voltammogram taken immediately prior. UV−vis spectra were recorded at 15 s intervals. When no further changes were observed, a reoxidizing potential of −0.3 to 0 V vs Ag was applied for between two and 5 min until the continuous UV−vis monitoring showed no further changes.

X-ray Crystallography. X-ray quality crystals of $[NBu_4]_2$[**1**], $[NBu_4]_2$[**2**]·0.25MeCN·0.25Et_2O and $[NBu_4]_2$[**3**] and $[NBu_4]_2$[**4**], and iodo-precursor $[NBu_4]_2$[**P2**]·Et_2O were grown by diffusion of diethyl ether into acetonitrile or acetone. Data were collected on a Rigaku XtalLab Synergy S diffractometer using a Photon-Jet Mo or Cu microfocus source and Hypix hybrid photon counting detector. Data reduction, cell refinement, and absorption correction were performed using Rigaku CrysAlisPro,[15] and the structure was solved with SHELXT[16] in Olex2 V1.5.[17] Refinement was achieved by full-matrix least-squares on all F_0^2 data using SHELXL (v. 2018−3),[18] also in Olex 2 V1.5. Full crystallographic data and refinement details are presented in Table S1 (in the Supporting Information) and ORTEP representations of the asymmetric units are provided in Figures S9−S13 (Supporting Information).

Hyper-Rayleigh Scattering. General details of the hyper-Rayleigh scattering (HRS) experiment have been discussed elsewhere,[19] and the experimental procedure and data analysis protocol used for the fs measurements used in this study were as previously described.[20] Measurements were carried out using dilute (ca. 10^{-5} M) filtered (Millipore, 0.45 μm) acetonitrile solutions, such that self-absorption of the second harmonic (SH) signal was negligible, verified by the linear relation between signal and concentration. The 1064 nm source was a Spectra-Physics InSight DS+ laser (1 W average power, sub-100 fs pulses, 80 MHz). The collection optics were coupled to a spectrograph (model Bruker 500is/sm), together with an EMCCD camera (Andor Solis model iXon Ultra 897). Correction for multiphoton fluorescence (MPF) was done by subtracting the broad MPF background signal from the narrow HRS peak (fwhm ± 9 nm). The high accuracy and sensitivity of this setup enable us to use the solvent as an internal reference (acetonitrile, $\beta_{HRS,1064}$ = 0.258 × 10^{-30} esu; $\beta_{zzz,1064}$ = 0.623 × 10^{-30} esu).[21] The depolarization ratio ρ for 2D compound $[NBu_4]_2$[**4**] was determined following established methods.[22] β tensor components β_{zzz} and β_{zyy} were extracted by assuming Kleinman and planar symmetry for C_{2v} molecules, yielding only two significant components of the β tensor, β_{zzz} and β_{zyy}. These are determined from orientationally averaged $\langle\beta_{HRS}^2\rangle$ and ρ by applying eqs 1 to 3[22c]

$$\begin{cases} \langle\beta_{HRS}^2\rangle = \langle\beta_{ZZZ}^2\rangle + \langle\beta_{YZZ}^2\rangle \\ \rho = \dfrac{\langle\beta_{ZZZ}^2\rangle}{\langle\beta_{YZZ}^2\rangle} \end{cases} \quad (1)$$

The HRS intensities with parallel polarization for fundamental and SH wavelengths, $\langle\beta_{ZZZ}^2\rangle$, and those for perpendicular polarization, $\langle\beta_{YZZ}^2\rangle$, can be expressed in terms of the molecular components β_{zzz} and β_{zyy} as follows

$$\begin{cases} \langle\beta_{ZZZ}^2\rangle = \dfrac{1}{7}\beta_{zzz}^2 + \dfrac{6}{35}\beta_{zzz}\beta_{zyy} + \dfrac{9}{35}\beta_{zyy}^2 \\ \langle\beta_{YZZ}^2\rangle = \dfrac{1}{35}\beta_{zzz}^2 - \dfrac{2}{105}\beta_{zzz}\beta_{zyy} + \dfrac{11}{105}\beta_{zyy}^2 \end{cases} \quad (2)$$

The depolarization ratio ρ can be expressed in terms of the ratio between the molecular β components, $k = \beta_{zyy}/\beta_{zzz}$.

$$\rho = \frac{15 + 18k + 27k^2}{3 - 2k + 11k^2} \quad (3)$$

This approach can also be applied to non-C_{2v} geometries in which case it produces *effective* values of the tensor components that give an indication of the dimensionality of β response.

Electrochemically switched HRS measurements were performed as described previously,[11] and further details are provided in the Supporting Information.

Quantum Chemical Calculations. Geometry optimizations were performed by density functional theory (DFT), using the range-separated ωB97X-D exchange-correlation functional (XCF)[23] with 6-311G(d)[24] (C, H, N, O) and LANL2TZ[25] (Mo) basis sets. Solvent effects (acetonitrile) were modeled using the integral equation formalism of the polarizable continuum model (IEF-PCM).[26] The reliability of the ωB97X-D/6-311G(d)/LANL2TZ method for the geometry optimization of POM derivatives was demonstrated in comparison with other XC functionals in a previous work.[7e] Excited-state properties were calculated for the optimized geometries using time-dependent density functional theory (TD-DFT),[27] with the same XCF, basis set, and IEF-PCM solvation. The 30 lowest excitation energies, oscillator strengths, and transition dipole moments μ_{ge} were calculated together with the ground-to-excited state dipole moment changes $\Delta\mu_{ge}$, charge transfer distances d_{CT} and amounts of charge transferred q_{CT}, according to the scheme presented by Le Bahers et al.[28] Again with the same optimized geometries, XCF,

https://doi.org/10.1021/acs.inorgchem.5c00915
Inorg. Chem. 2025, 64, 8408−8420

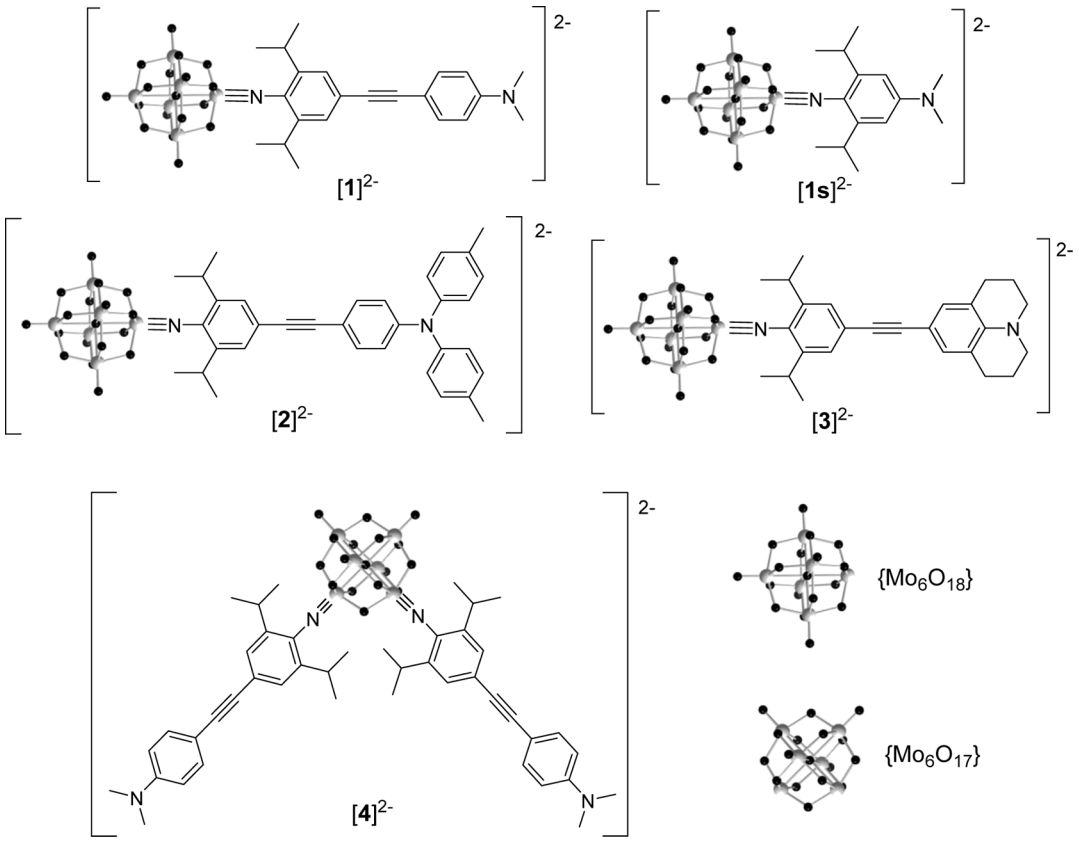

Figure 1. Structures of complex anions $[\mathbf{1}]^{2-}$ to $[\mathbf{4}]^{2-}$ synthesized for this study and previously published[11] $[\mathbf{1s}]^{2-}$ included for comparison. All compounds were isolated as tetrabutylammonium salts.

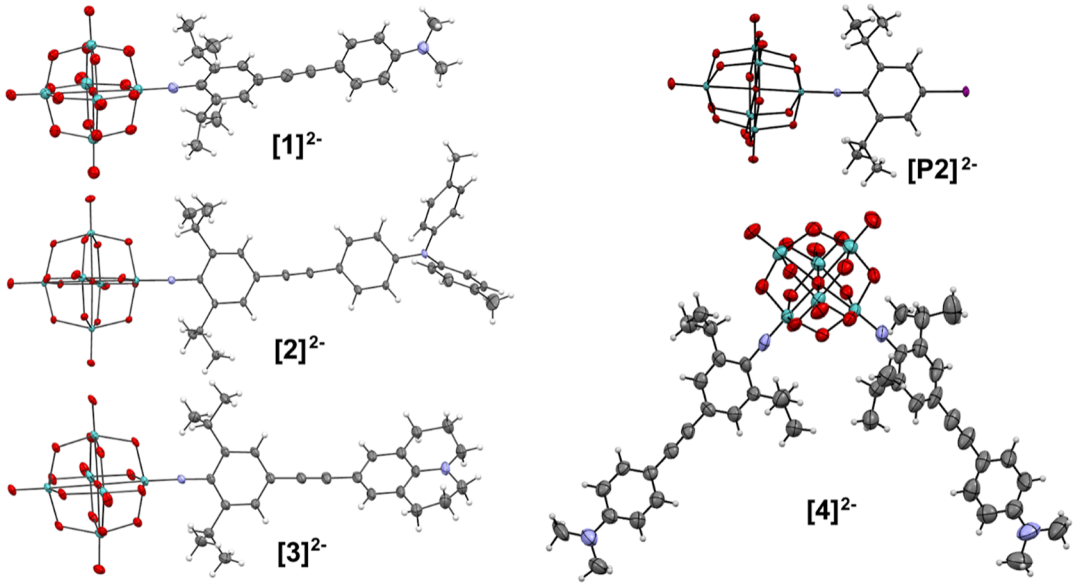

Figure 2. ORTEP representations of the complex anions in $[NBu_4]_2[\mathbf{P2}]$ and $[NBu_4]_2[\mathbf{1}]$ to $[NBu_4]_2[\mathbf{4}]$. Thermal ellipsoids are drawn at the 30% probability level. Disorder in the julolidinyl group of $[\mathbf{3}]^{2-}$ has been omitted for clarity but is shown in Figure S12 (Supporting Information). Color scheme: C is gray; N, purple; O, red; Mo, green; I, purple. H atoms are represented by white spheres of arbitrary radii.

basis set, and IEF-PCM scheme, SHG β tensor components were evaluated using the quadratic response TD-DFT method:[29] ωB97X-D has been shown to be a reliable XCF for calculating the β tensors owing to its substantial amount of long-range HF exchange.[30] Both static and dynamic (incident wavelength of 1064 nm) responses were calculated. For 2D anion $[\mathbf{4}]^{2-}$, the molecular response has been analyzed using the computed depolarization ratios and assuming Kleinman symmetry to obtain the two components β_{zzz} and β_{zyy}, as described above for the HRS results. Further details of all computational aspects are provided in the Supporting Information.

RESULTS AND DISCUSSION

Chromophore Design and Synthesis. Anions $[\mathbf{1}]^{2-}$ to $[\mathbf{4}]^{2-}$ (Figure 1) were designed to test the effects of donor type

https://doi.org/10.1021/acs.inorgchem.5c00915
Inorg. Chem. 2025, 64, 8408−8420

and chromophore geometry in isopropyl-protected arylimido hexamolybdate derivatives. In the linear series, these comprise a moderately strong resonance electron donor ($-NMe_2$, $[\mathbf{1}]^{2-}$), a weakened resonance electron donor that allows delocalization of charge onto an electron-rich aromatic ($-NTol_2$, $[\mathbf{2}]^{2-}$), and a very strong resonance electron donor (julolidinyl, Jd, $[\mathbf{3}]^{2-}$), which has previously yielded very high NLO activities in organic charge transfer (CT) chromophores.[31] V-shaped (C_{2v}) *bis*-imido derivative $[\mathbf{4}]^{2-}$ features the $-NMe_2$ donor. The four compounds were obtained as their tetrabutylammonium salts by first synthesizing the required *mono*- or *bis*-(iodoarylimido) polyoxometalate derivatives $[NBu_4]_2[\mathbf{P2}]$ and $[NBu_4]_2[\mathbf{P3}]$ from tetrabutylammonium hexamolybdate using a well-established DCC-mediated imido coupling.[7,11,32] We tested alternative, potentially more efficient syntheses of the *bis*-arylimido-functionalized anion $[\mathbf{P3}]^{2-}$ starting from $[Mo_8O_{26}]^{4-}$,[33] but in our hands, these yielded inseparable mixtures of products. Subsequently, Sonogashira protocols were used to attach the required donor group via an alkyne bridge (Scheme S1, Supporting Information).[7ac,33,33] Identity and purity of the chromophores were confirmed using ^{1}H NMR, ^{13}C NMR, mass spectrometry, CHN analysis, and IR and UV−vis spectroscopy, and structures (including the *cis* substitution pattern in $[\mathbf{4}]^{2-}$) were also confirmed by X-ray diffraction.

^{1}H NMR analysis of the *mono*-donor series (Figures S1−S3, Supporting Information) showed chemical shifts for the aromatic protons closest to the POM of 7.25 ppm for $[\mathbf{1}]^{2-}$, 7.28 ppm for $[\mathbf{2}]^{2-}$, and 7.20 ppm for $[\mathbf{3}]^{2-}$, consistent with the expected trend for the strength of the electron donors, with $-NTol_2$ ($[\mathbf{2}]^{2-}$) shielding the protons least and Jd ($[\mathbf{3}]^{2-}$) shielding the most. Similarly, for $[\mathbf{4}]^{2-}$ (Figure S4), these protons are slightly more shielded (7.23 ppm) than for $[\mathbf{1}]^{2-}$ as *bis* functionalization of the POM core results in weaker electron withdrawal from the individual ligands by the POM. Similar but weaker effects are observed on the isopropyl CH_3 protons of the four compounds.

X-ray Crystallography. X-ray quality crystals were obtained for all four compounds and the precursor polyoxometalate $[NBu_4]_2[\mathbf{P2}]$, from ether diffusion into either acetone or acetonitrile solutions, enabling determination of crystal structures (Figures 2 and S9−S13 and Tables S1 and S2, Supporting Information). These confirm the *cis*-geometry of $[NBu_4]_2[\mathbf{4}]$: both dipolar (C_{2v}) *cis*- and centrosymmetric, quadrupolar *trans*-isomers of *bis*-substituted imido-Lindqvist species are possible,[34] but show centrosymmetric (i.e., bulk SHG inactive) space groups for all compounds. Mo−O and Mo−N bond lengths (Table S2) of $[NBu_4]_2[\mathbf{P2}]$ and $[NBu_4]_2[\mathbf{1}]$ to $[NBu_4]_2[\mathbf{3}]$ are comparable to those seen for previous derivatized $\{Mo_6\}$ clusters, and while there is no significant trend in the length of the imido bonds, all three did show the increased linearity seen of previously published compounds featuring ^{i}Pr groups adjacent to the imido bond, as steric repulsion between ^{i}Pr and the POM restricts deviation of the Mo−N−C angle from 180°. Relatively low precision on bond lengths of $[\mathbf{1}]^{2-}$ and $[\mathbf{4}]^{2-}$ precludes in depth comparison of the structures of the π-bridges in this study and with those of prior derivatives, but it is worth noting that data obtained for *bis*-derivative $[NBu_4]_2[\mathbf{4}]$ do not indicate substantial differences to the bond lengths and angles observed for the *mono* analogue $[NBu_4]_2[\mathbf{1}]$. The low-energy barriers of rotation in unhindered phenylacetylenes (ca. 1 kcal mol^{-1})[35] result in both twisted and planar arrangements in crystal structures; however, previous crystallographic work has determined a pattern of increasingly planarity with weaker donor groups, ascribed to stronger conjugation in systems with less charge asymmetry.[7b] Here, a similar trend is observed, with twist around the alkyne bond smallest in $[\mathbf{2}]^{2-}$, the weakest donor, and largest in $[\mathbf{3}]^{2-}$, the strongest donor. The average twist observed for the two donor arms of $[\mathbf{4}]^{2-}$ is very similar to that of $[\mathbf{1}]^{2-}$. Compared to previously published analogues with H atoms *ortho* to the imido groups instead of ^{i}Pr, $[\mathbf{1}]^{2-}$ to $[\mathbf{4}]^{2-}$ all show a much less twisted diphenylacetylene bridge—for example, the 2,6-H analogue of $[\mathbf{1}]^{2-}$ shows a torsion angle of 86° vs 17.6° observed here. This suggests that the more linear imido bonds of the sterically protected compounds lead to increased conjugation through the π-bridge, although the influence of different crystal packing effects cannot be excluded.

Electronic Spectroscopy and Electrochemistry. UV−vis absorption spectra of $[NBu_4]_2[\mathbf{1}]$ to $[NBu_4]_2[\mathbf{4}]$ (Figure 3 and Table 1) all revealed Mo−O and $\pi-\pi^*$ peaks in the 200−300 nm region, with the higher peak extinction coefficients of $[NBu_4]_2[\mathbf{4}]$ a consequence of the second ligand—although notably, the absorption of this compound tails off rapidly so that there is no more absorption at the 532 nm second harmonic wavelength than for the other *mono*-derivatives. In addition, ligand-to-POM charge transfer (LPCT) peaks were seen in the 420−455 nm range for all four compounds. Compared to its phenyl-bridged analogue $[NBu_4]_2[\mathbf{1s}]$,[11] the LPCT peak of compound $[NBu_4]_2[\mathbf{1}]$ shows a blue shift, from 431 to 424 nm. Commonly, extending conjugation red shifts CT transitions, but in arylimido-POMs with strong donors ($-NMe_2$ and $-NPh_2$), we have seen the opposite when a phenyl bridge is replaced by diphenylacetylene.[7d] This is likely a consequence of weakened electronic communication due to free rotation around the alkyne bond, which reduces the extent of charge transfer onto the POM core. Spectrally, $[NBu_4]_2[\mathbf{1}]$ and $[NBu_4]_2[\mathbf{2}]$ are very similar, with only a 1 nm blue shift of the LPCT peak of compound **2** from 424 to 423 nm despite the slight decrease in donor strength. Larger blue shifts were previously observed on changing $-NMe_2$ for $-NPh_2$,[7c] showing that the methyl groups in $-NTol_2$ result in stronger

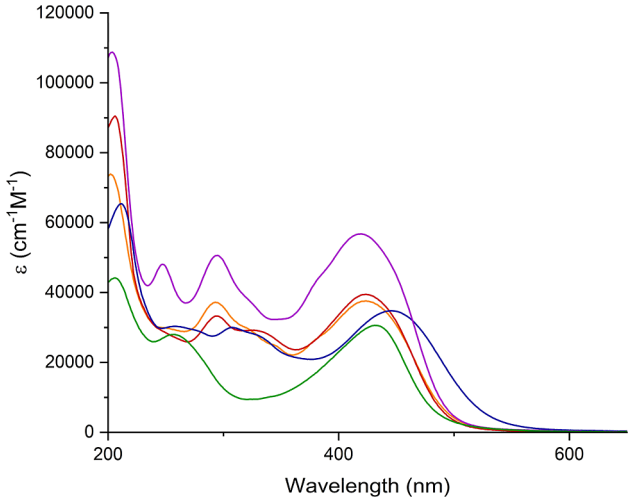

Figure 3. UV−vis spectra of compound $[NBu_4]_2[\mathbf{1}]$ (orange), $[NBu_4]_2[\mathbf{2}]$ (red), $[NBu_4]_2[\mathbf{3}]$ (blue), $[NBu_4]_2[\mathbf{4}]$ (purple), and $[NBu_4]_2[\mathbf{1s}]$ (green) obtained in acetonitrile.

https://doi.org/10.1021/acs.inorgchem.5c00915
Inorg. Chem. 2025, 64, 8408−8420

Table 1. UV−Vis Absorption and Electrochemical Data for the Oxidized and Reduced States of Compounds 1, 2, and 3 in Acetonitrile[d]

	λ_{max}/nm[a] (ε, 10^3 M^{-1} cm^{-1})	E_{max}/eV	E/V vs Fc/Fc^+ (ΔE_p/mV)[b]		
			E_{pc} $[X]^{3-/4-}$	$E_{1/2}$ or E_{pc} $[X]^{2-/3-}$	E_{pa} $[X]^{n/2-}$
$[\mathbf{1}]^{2-}$	203 (73.6)	6.11	−1.837	−1.013 (85)	0.338 irr
	293 (37.1)	4.23			
	424 (37.6)	2.92			
$[\mathbf{1}]^{3-}$	202 (71.8)	6.14			
	296 (34.6)	4.19			
	406 (45.9)	3.05			
$[\mathbf{2}]^{2-}$	206 (90.4)	6.02	−1.905	−1.009 (73)	0.493 quas
	294 (33.1)	4.22			
	329 (19.0)	3.77			
	423 (39.4)	2.93			
$[\mathbf{2}]^{3-}$	204 (96.4)	6.08			
	296 (34.6)	4.19			
	406 (48.7)	3.05			
$[\mathbf{3}]^{2-}$	212 (65.3)	5.85	−1.831	−1.020 (85)	0.119 irr
	259 (30.3)	4.79			
	308 (30.0)	4.03			
	445 (37.8)	2.79			
$[\mathbf{3}]^{3-}$	210 (68.0)	5.90			
	308 (29.2)	4.03			
	414 (42.4)	2.99			
$[\mathbf{4}]^{2-}$	204 (108.7)	6.08		−1.056[c]	
	246 (48.1)	5.04			
	295 (50.6)	4.20			
	420 (56.7)	2.95			

[a]UV−vis data for $[\mathbf{1/2/3/4}]^{2-}$ were obtained from ca. 10^{-5} M solutions in MeCN. UV−vis data for $[\mathbf{1/2/3}]^{3-}$ were obtained from ca. 10^{-2} M solutions in 0.3 M $[NBu_4][BF_4]$ using a thin layer spectroelectrochemistry cell, with ε for $[\mathbf{1/2/3}]^{2-}$ prior to reduction used to determine concentration. [b]Analyte concentrations ca. 10^{-3} M in 0.1 M $[NBu_4][BF_4]$ in MeCN glassy carbon working electrode, scan rate of 100 mV s^{-1}. [c]E_{pc}, $[\mathbf{4}]^{3-}$ is unstable on the CV time scale. [d]UV−vis Absorption and electrochemical data of compound **4** is included for the oxidized state only.

electron donation. The LPCT peak of the julolidinyl derivative $[NBu_4]_2[\mathbf{3}]$ (445 nm) was red-shifted compared to $[NBu_4]_2[\mathbf{1}]$ and $[NBu_4]_2[\mathbf{2}]$ due to the stronger donor group, decreasing the transparency. The LPCT peak of $[NBu_4]_2[\mathbf{4}]$ is blue-shifted 4 nm from $[NBu_4]_2[\mathbf{1}]$, suggesting that addition of a second donor unit weakens the donor−acceptor character of the transition, by weaking the acceptor strength of the POM as reflected in a more negative redox potential for the first reduction (vide infra).

Cyclic voltammograms (Table 1 and Figure S14) of *mono*-derivatives $[NBu_4]_2[\mathbf{1}]$ to $[NBu_4]_2[\mathbf{3}]$ revealed $[Mo_6O_{18}NAr]^{2-/3-}$ reduction peaks with near ideal reversibility and slight shifts in redox potential consistent with donor strength—the shifts are small as the diphenylethyne bridge (compared to phenyl) gives a degree of electronic isolation between the donor and POM core.[7b] Logically, the irreversible or weakly reversible donor oxidations occurred at less positive potential for compounds with stronger donors, with oxidation of $[\mathbf{3}]^{2-}$ (Jd) occurring more than 380 mV more negative than $[\mathbf{2}]^{2-}$ (−$NTol_2$). Reduction of $[\mathbf{4}]^{2-}$ (Figure S15) did not find the reversible $[Mo_6O_{18}NAr]^{2-/3-}$ reduction typically seen of hexamolybdate derivatives, with the quasi-reversible $[Mo_6O_{17}(NAr)_2]^{2-/3-}$ reduction peak showing that significant decomposition occurred even at fast scan rates. Moreover, no $[Mo_6O_{19}]^{2-/3-}$ peaks emerged, suggesting that decomposition of $[\mathbf{4}]^{2-}$ does not proceed through the solvolysis pathway observed for analogues without steric protection.[11,36]

However, study of $[NBu_4]_2[\mathbf{1}]$ to $[NBu_4]_2[\mathbf{3}]$ by bulk electrolysis revealed greatly improved stability compared to previous compounds without ^{i}Pr groups:[7,11,36] after 23 min bulk electrolysis (near complete reduction), 83% of $[\mathbf{2}]^{2-/3-}$ remained and 75% of $[\mathbf{1}]^{2-/3-}$ and $[\mathbf{3}]^{2-/3-}$ (Figure S16)—compared to typically no more than 20% of compounds with only H in the 2 and 6 positions of the imido ring. Thus, the steric bulk of the ^{i}Pr groups appears to be effective in protecting the imido bond from solvent or adventitious water. Interestingly, post-electrolysis cyclic voltammetry showed no signal for $[Mo_6O_{19}]^{2-/3-}$ suggesting, as for $[\mathbf{4}]^{3-}$, decomposition was not occurring via the expected solvolysis pathway, and no other new electrochemically active species were observed. This suggested breakdown of $\{Mo_6\}$ to form other isopolyoxometalate species, many of which, as compounds with *cis*-terminal dioxo groups, show only destructive redox processes at highly negative potentials that can overlap with solvent reduction.[37] IR analysis of a sample of $[\mathbf{1}]^{2-/3-}$ through a bulk electrolysis (Figure 4) showed emergence of new peaks

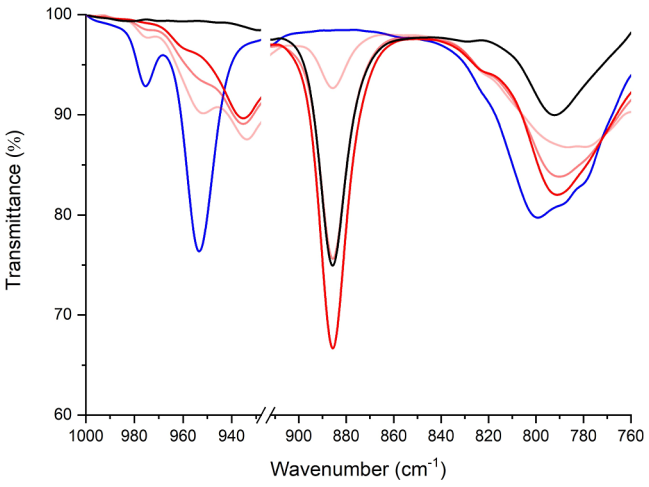

Figure 4. IR spectra of $[NBu_4]_2[\mathbf{1}]$ taken before (blue) and during (darkening red) with the spectra of $[Mo_2O_7]^{2-}$ included (black) for comparison. All spectra were obtained in MeCN solution with supporting electrolyte 0.1 M $[NBu_4][BF_4]$.

at ca. 885 cm^{-1} and 790 cm^{-1} consistent with the presence of $[Mo_2O_7]^{2-}$ and decomposition via fragmentation of the POM core, potentially after departure of a {MoNAr} subunit. Fragmentation of the hexamolybdate core of organoimido derivatives to smaller Mo-containing species including $HMo_2O_7^-$ and {MoNAr} units has previously been observed in MS−MS experiments—most of all, for a system where the Ar unit carried a resonance (−OMe) donor.[38] It is likely similar pathways are also responsible for the lower stability of $[\mathbf{4}]^{3-}$ and are encouraged by imido functionalization. Thus, slowing the hydrolysis/solvolysis pathway using steric bulk reveals slower decomposition pathways for the reduced $\{Mo_6\}$ unit that may be a result of increased charge asymmetry on the cluster due to the electron-donating imido fragment. In previously published phenyl-bridged, ^{i}Pr-protected $[NBu_4]$-

https://doi.org/10.1021/acs.inorgchem.5c00915
Inorg. Chem. 2025, 64, 8408−8420

[1s],[11] this type of decomposition was much less evident, suggesting that the extended conjugated ligands play a role in enabling it—possibly by stabilizing or helping solvate the proposed {MoNAr} subunits. In future work, the stability of the reduced states may be improved by using noncoordinating, water-immiscible solvents—for example, dichloromethane—although the increased resistance of such generally less polar media can be a challenge in electrochemical experiments. The ideal solvent for redox-switching in solution would be highly polar, but noncoordinating, water-immiscible, and low viscosity.

Study of the reduced anions $[\mathbf{1}]^{3-}$ to $[\mathbf{3}]^{3-}$by UV−vis spectroelectrochemistry (Figures 5 and S17) revealed a ca. 17

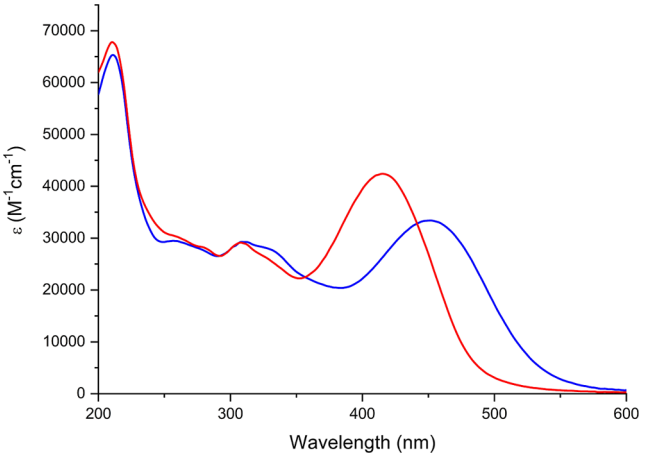

Figure 5. UV−vis spectra of $[\mathbf{3}]^{2-}$ (blue) and $[\mathbf{3}]^{3-}$ (red) obtained by spectroelectrochemistry (electrolyte 0.3 M NBu_4BF_4 in dry MeCN). A 97% recovery of the original spectrum was revealed upon reoxidation.

nm blue shift of the LPCT peaks of $[\mathbf{1}]^{3-}$ and $[\mathbf{2}]^{3-}$ relative to the parent dianions, and this increased to 31 nm for $[\mathbf{3}]^{3-}$. This shows that reduction of the POM anion lessens its ability as an electron acceptor, increasing the energy of the LPCT transition. A similar shift was previously observed for $[\mathbf{1s}]^{2-/3-}$, which showed reversible switching of the second-order NLO response.[11] The change in the spectrum was reversible for all three *mono*-functionalized compounds, with 98% recovery of the absorbance of the LPCT peak for $[NBu_4]_2[\mathbf{2}]$ and 97% recovery for $[NBu_4]_2[\mathbf{1}]$ and $[NBu_4]_2[\mathbf{3}]$.

Hyper-Rayleigh Scattering. Hyper-Rayleigh Scattering measurements performed at 1064 nm were used to investigate the NLO activity of $[NBu_4]_2[\mathbf{1}]$ to $[NBu_4]_2[\mathbf{4}]$, including depolarization measurements to determine the β components of $[NBu_4]_2[\mathbf{4}]$ (Table 2). Similar to previous studies with POMophores,[7b] extending from phenyl-bridged $-NMe_2$ donor $[\mathbf{1s}]^{2-}$ to phenylacetylene $[\mathbf{1}]^{2-}$ substantially enhances the response (close to 100%) while producing a blue shift rather than red shift in λ_{max}. Changing to the $-NTol_2$ donor $[\mathbf{2}]^{2-}$ increases β-values further, as previously observed for $-NPh_2$,[7c,d] due to the extension of the HOMO onto the aryl groups, increasing ground-to-excited state dipole moment changes $\Delta\mu$, and also the extension of the π-system strengthening communication right across the bridge. Both $[\mathbf{1}]^{2-}$ and $[\mathbf{2}]^{2-}$ show an increase (ca. 15%) in NLO activity over similar compounds without steric protection.[7b,c] This should be treated with caution, as it is within typical HRS measurement errors, but is consistent with the possibility that increased linearity of the Mo−N-Aryl linkage imposed by the ^{i}Pr groups, and resulting strengthened communication through the π-system (suggested by smaller twist angles across the alkyne bond), plus increased electron density of the π-system due to the inductive effect of ^{i}Pr, may be leading to increased β. Maximizing the electron donor strength with the julolidinyl group in $[\mathbf{3}]^{2-}$ produced the highest NLO activity of any POM chromophore to date, with a 10% increase in $\beta_{0,zzz}$ and only a 7 nm increase in λ_{max} over a system with a stilbene bridge and $-NPh_2$ donor.[7d] This reveals maximizing donor strength, with ^{i}Pr groups to control the imido-geometry and a diphenylacetylene bridge as an attractive approach to increasing β in POMophores, as synthetically such systems are more straightforward to access than stilbene-derivatized POMs.

Comparison of $\beta_{HRS,0}$ of compound $[\mathbf{4}]^{2-}$ to that of monofunctionalized analogue $[\mathbf{1}]^{2-}$ reveals a 22% increase in orientationally averaged $\beta_{0,HRS}$, from 68×10^{-30} esu to 83×10^{-30} esu. Combined with a decrease in λ_{max}, this gives an excellent combination of activity and transparency. Measurement of a depolarization ratio and extraction of β_{zzz} and β_{zyy} tensor components reveals only a relatively minimally 2-dimensional response: $\beta_{zyy,0}$, at -26.6×10^{-30} esu is only a little more than 10% of $\beta_{zzz,0}$, likely a result of the relatively tight D···A···D angle of 90°. Nonetheless, this result shows

Table 2. Experimental Values of Hyperpolarizability, β for $[NBu_4]_2[\mathbf{1}]$ to $[NBu_4]_2[\mathbf{4}]$, and $[NBu_4]_2[\mathbf{1s}]$ Measured by Hyper-Rayleigh Scattering in Acetonitrile[a]

	LPCT λ_{max} (nm)	$\beta_{HRS,1064}$[b] ($\times 10^{-30}$ esu)	$\beta_{HRS,0}$[c] ($\times 10^{-30}$ esu)	ρ	$\beta_{zzz,1064}$ ($\times 10^{-30}$ esu)	$\beta_{zzz,0}$ ($\times 10^{-30}$ esu)	$\beta_{zyy,1064}$ ($\times 10^{-30}$ esu)	$\beta_{zyy,0}$ ($\times 10^{-30}$ esu)
$[NBu_4]_2[\mathbf{1}]$	424	220	68	n.d.	531[d]	162[f]	n.d.	n.d.
$[NBu_4]_2[\mathbf{1s}]$	431	128	37	n.d.	309[d]	89[f]	n.d.	n.d.
$[NBu_4]_2[\mathbf{2}]$	423	297	92	n.d.	717[d]	222[f]	n.d.	n.d.
$[NBu_4]_2[\mathbf{3}]$	445	532	132	n.d.	1285[d]	318[f]	n.d.	n.d.
$[NBu_4]_2[\mathbf{4}]$	420	260	83	3.83	654[e]	208[g]	−83.3[e]	−26.6[g]

[a]Data for $[NBu_4]_2[\mathbf{1s}]$ are taken from ref 11. [b]Total molecular HRS response measured using 1064 nm fundamental laser beams. The quoted units (esu) can be converted into SI units ($C^3\ m^3\ J^{-2}$) by dividing by a factor of 2.693×10^{20}. [c]Nonresonant, static β estimated from β_{HRS} using the two-state model.[39] [d]Dynamic β_{zzz} derived assuming a single dominant tensor component due to linear, dipolar symmetry. [e]Dynamic β tensor components derived from the HRS intensity and depolarization ratio, ρ. [f]Static β_{zzz} derived assuming a single dominant tensor component due to linear, dipolar symmetry. [g]Static β tensor components derived from the HRS intensity and depolarization ratio, ρ. Note that ρ for $[NBu_4]_2[\mathbf{4}]$ is high enough to be treated using a two-state model and a single dominant tensor component, yielding $\beta_{zzz,0} = 192 \times 10^{-30}$ esu with all other components zero.

https://doi.org/10.1021/acs.inorgchem.5c00915
Inorg. Chem. 2025, 64, 8408−8420

Table 3. TD-DFT-Computed Electronic Transitions, 1064 nm and Static β Responses for $[NBu_4]_2[1]$ to $[NBu_4]_2[4]$ and $[NBu_4]_2[1s]$ in Acetonitrile[a]

	LPCT λ_{max}[b]/nm	LPCT E_{max}[b] (f)/eV	$\beta_{HRS,1064}$[c]/10^{-30} esu	$\beta_{zzz,1064}$[c]/10^{-30} esu	$\beta_{zyy,1064}$[c]/10^{-30} esu	$\beta_{HRS,0}$[d]/10^{-30} esu	$\beta_{zzz,0}$[d]/10^{-30} esu	$\beta_{zyy,0}$[d]/10^{-30} esu
$[1]^{2-}$	388	3.20 (1.98)	175	424[e]	n.d.	66.2	160[e]	n.d.
$[1]^{3-}$	354	3.50 (1.93)	11.7	28.2[e,f]		36.4	88.0[e]	
$[1s]^{2-}$	393	3.16 (1.02)	73.9	178[e]	n.d.	28.6	69.1[e]	n.d.
$[1s]^{3-}$	369	3.36 (0.98)	45.8	111[e]		22.8	55.0[e]	
$[2]^{2-}$	386	3.21 (2.25)	178	430[e]	n.d.	66.7	161[e]	n.d.
$[2]^{3-}$	358	3.46 (2.25)	10.8	26.1[e,f]		34.3	82.7[e]	
$[3]^{2-}$	397	3.12 (2.06)	245	593[e]	n.d.	85.2	206[e]	n.d.
$[3]^{3-}$	360	3.44 (1.95)	33.3	80.3[e,f]		47.3	114[e]	
$[4]^{2-}$	393	3.15 (2.08)	213	528[g]	−38.3[g]	80.4	194[g]	−19.6[g]
	376	3.30 (1.68)						
$[4]^{3-}$	379	3.27 (1.22)	112	277[g]	−19.2[g]	46.1	111[g]	−14.1[g]
	378	3.28 (0.34)						
	352	3.52 (1.50)						
	350	3.54 (0.31)						

[a]All calculations carried out by TD-DFT at the ωB97X-D/6-311G(d)/LanL2TZ level of theory with acetonitrile solvation by IEFPCM. β-Values are reported following B-convention to facilitate comparison with experiment. [b]Vertical transitions. [c]Dynamic HRS β responses, calculated at 1064 nm. [d]Static response extracted from calculations at λ = 1500 nm, to avoid resonance effects. [e]β_{zzz} calculated assuming a single dominant tensor component. [f]Large difference vs $[X]^{2-}$ state is a consequence of resonance effects. [g]Tensor components deduced from computed ρ and β_{HRS} values, assuming planar C_{2v} symmetry. Alternative treatment of $[4]^{2-}$ assuming a single dominant tensor component yields $\beta_{zzz,1064} = 513 \times 10^{-30}$ esu with all other components zero.

promise for 2D D···A···D POMophores in increasing β without extending visible absorption profiles.

The large blue shift in linear absorption obtained for $[NBu_4]_2[3]$ upon reduction (vide supra) implies a significant change in nonlinear optical properties, and as the compound with the highest oxidized state $\beta_{0,zzz}$, it was decided to investigate the electrochemical switching of the HRS response for this compound. Reduction produced a 60% decrease in the intensity of the second harmonic scattered light over 400 seconds (Figure S18, Supporting Information). However, no plateau of the HRS signal intensity could be obtained, suggesting an ongoing degradation process forming byproducts with low, or zero activity, as well as the electrochemical reduction. Reoxidation restored 90% of the NLO activity of the sample, indicating that the NLO responses can be switched on and off, but combined with the bulk electrolysis data, it shows that $[3]^{3-}$ is not sufficiently stable for multiple cycles under these conditions.

DFT and TD-DFT Calculations. DFT and TD-DFT calculations were performed on anions $[1]^{2-}$ to $[4]^{2-}$ and their reduced states in Gaussian 2016 at the ωB97X-D, 6-311G(d)/LanL2TZ, IEF-PCM(acetonitrile) level of theory. Computed geometries (Table S3, Supporting Information) of the oxidized states generally show a good agreement with the experimentally determined X-ray crystal structures. Experimental data for the $[X]^{3-}$ reduced-state structures is not available, but trends in computed oxidized and reduced-state electronic absorption spectra (vide infra) are a good match for spectroelectrochemical findings. The electronic structures (Figures S19−S23, Supporting Information) show for the oxidized states of all compounds a HOMO based on the ligand(s) and imido-group and a LUMO delocalized across the POM. Similar to previous findings for $[1s]^{3-}$, for the reduced monodonor compounds $[1]^{3-}$ to $[3]^{3-}$, a spin-α HOMO−1 is found based on the POM, between 0.06 (−NMe_2 donor $[1]^{3-}$) and 0.31 eV (Jd donor $[3]^{3-}$) lower in energy than a closely spaced pair of donor/aryl-imido-based HOMOs (one spin-α, one spin-β). In the reduced *bis*-donor system $[4]^{3-}$, the increased electron density on the POM lifts the POM-based spin-α SOMO to higher energy than a group of four ligand-based HOMO/HOMO-x orbitals (spin-α and spin-β, located on each ligand). Spin-density calculations for the compounds indicate that the spin is either largely, or entirely located on the POM anions (Figure S24).

For the oxidized, monodonor species $[1]^{2-}$ to $[3]^{2-}$, trends in the TD-DFT computed vertical transition energies (Table 3 and Figure S25) match experimental observations—the red shift for the strong julolidinyl donor is smaller than observed experimentally, but vertical transition energies do not account for geometry relaxation of the excited state, or vibronic structure, that are pertinent to experimental measurements. The red, rather than experimentally observed blue shift in the lowest energy transition of V-shaped anion $[4]^{2-}$ compared to $[1]^{2-}$ is likely to be a result of the two bands (3.15 and 3.30 eV) overlapping in the experimental spectrum so that the peak is seen at higher energy. In all cases, calculated charge transfer vectors and changes in electron density distribution ($\Delta\rho$) indicate CT from the arylimido ligands, toward the polyoxometalate, with increases in electron density at the POM and decreases on the donor (Figures 6 (left), S26, and S27); however, compared to previously studied analogues without isopropyl groups,[7e] dipole moment changes $\Delta\mu_{ge}$ and charge transfer distances d_{CT} (Table S4) for $[1]^{2-}$ and $[2]^{2-}$ are lower, likely because the acceptor ring and POM are more electron rich. The powerful Jd donor group, however, gives the highest $\Delta\mu_{ge}$ yet computed for an arylimido-POM, consistent with its high β-value.

Consistent with experiment, the computed LPCT UV−vis absorption bands of the reduced-state spectra ($[1]^{3-}$ to $[3]^{3-}$) show blue shifts (Table 3 and Figure S28), versus the oxidized states. Weaker, low-energy peaks in the computed spectra are at energies consistent with reported experimental spectra for $[Mo_6O_{19}]^{3-}$,[40] concentrations used in spectroelectrochemical measurements were too low for detection of these peaks, which may be merged with the absorption tail of the LPCT band. Similar to the experimental data, the largest blue shift is

https://doi.org/10.1021/acs.inorgchem.5c00915
Inorg. Chem. 2025, 64, 8408−8420

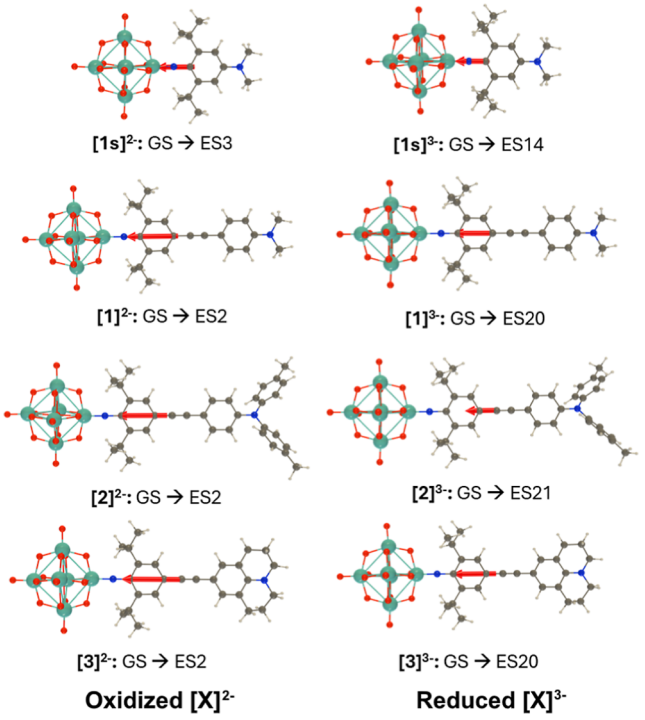

Figure 6. Charge transfer vectors (from the negative to the positive barycenter of $\Delta\rho$) upon excitation from GS to the nth ES of the oxidized and reduced states of the 1-D anions $[\mathbf{1s}]^{2-/3-}$ and $[\mathbf{1}]^{2-/3-}$ to $[\mathbf{3}]^{2-/3-}$, as evaluated at the IEF-PCM(acetonitrile)/TDDFT/ωB97X-D/6-311G(d)/LanL2TZ level. The nonequilibrium solvation approach was adopted.

observed for $[\mathbf{3}]^{3-}$ vs $[\mathbf{3}]^{2-}$; however, the computed blue shifts are generally larger than those observed by experiment. This, and the tendency of experimental ε values to increase upon reduction, while computed oscillator strengths decrease slightly, is likely a consequence of differences in geometry relaxation and vibronic structure between the oxidized and reduced states, which are not captured by the calculation. Computed charge transfer vectors (Figures 6 and S26), dipole moment changes (Table S4), and changes in electron density (Figures S19 and S27) show that CT is still from the ligand to POM, but less strongly, with $\Delta\mu_{ge}$ dropping more dramatically from $[\mathbf{X}]^{2-}$ to $[\mathbf{X}]^{3-}$ state for the new, extended systems $[\mathbf{1}]^{2-/3-}$ to $[\mathbf{4}]^{2-/3-}$ than for previously studied, phenyl-bridged $[\mathbf{1s}]^{2-}$.

Computed dynamic first hyperpolarizabilities $\beta_{HRS,1064}$ and $\beta_{zzz,1064}$ of the oxidized species (Table 3) follow experimental trends in finding that of the phenylacetylene-bridged systems $[\mathbf{1}]^{2-}$ to $[\mathbf{4}]^{2-}$, *mono*-NMe_2 donor $[\mathbf{1}]^{2-}$ has the lowest activity, and julolidinyl derivative $[\mathbf{3}]^{2-}$ the highest. Generally, similar to previous studies, the computed values are lower than those found experimentally, most notably for $[\mathbf{2}]^{2-}$ and $[\mathbf{3}]^{2-}$. In the case of $[\mathbf{3}]^{2-}$, it is possible that the more red-shifted absorption profile leads to an increased resonance contribution to the experimental result, but the computed value still represents a new record for a POMophore. For $[\mathbf{2}]^{2-}$, there is no red-shift vs $[\mathbf{1}]^{2-}$, but we have noted previously that computed β-values tend to be underestimated for $-NAr_2$ donors with diphenylacetylene and stilbene bridges. As found by experiment, adding a second donor arm ($[\mathbf{4}]^{2-}$ vs $[\mathbf{1}]^{2-}$) yields a ca. 20% increase in activity (orientationally averaged β_{HRS}), and computationally determined tensor components β_{zzz} and β_{zyy} for this C_{2v} anion are similar to experiment in showing only very minimal 2D character in the response, which can be adequately described by a single tensor component β_{zzz}. Computed static hyperpolarizabilities β_0 are also shown in Table 3, extracted from values calculated at 1500 nm, away from resonance effects. Generally, these are closer in magnitude to experimental values than the dynamic 1064 nm ones and follow experimental trends, although values for $-NTol_2$ and Jd donors are comparatively underestimated.

In addition to the oxidized species, hyperpolarizabilities have been calculated for the reduced states $[\mathbf{X}]^{3-}$. These show that in all cases, the increase in CT transition energies caused by reduction of the POM feeds through into lowered β values. Decreases in β_0 are around 50%, as signal intensity is proportional to β^2, this would be consistent with a 75% decrease in signal intensity in the absence of resonance effects. Larger changes computed for β_{1064} in $[\mathbf{1}]^{2-/3-}$ to $[\mathbf{3}]^{2-/3-}$ result from resonance effects that may not be experimentally observed—depending on the accuracy of computed absorption profiles—and are not pertinent to all wavelengths. Thus, the experimental 60% decrease in signal obtained for reduction of $[\mathbf{3}]^{2-}$ to $[\mathbf{3}]^{3-}$ is consistent with the calculated changes in β. The origin of the decreased β values is primarily the smaller (by up to 45%) $\Delta\mu_{ge}$ found for the reduced states, and the effect of this on the β tensors is graphically represented for $[\mathbf{3}]^{2-/3-}$ (Figure 7) and the other compounds (Figure S30) in

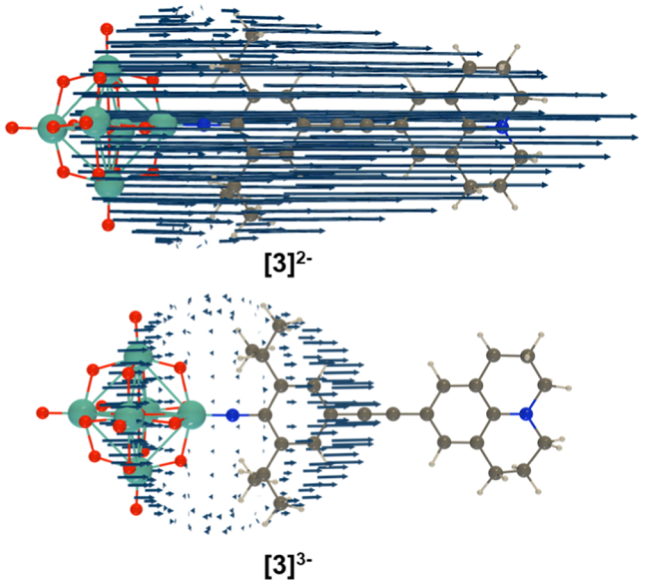

Figure 7. Unit sphere representation (USR) of the first hyperpolarizability tensor (λ = 1064 nm) of $[\mathbf{3}]^{2-}$ and $[\mathbf{3}]^{3-}$ as calculated at the IEFPCM (solvent = acetonitrile) TDDFT/wB97X-D/6-311G(d)/LanL2TZ level of approximation. Factor = 10^{-4} Å/a.u.$_\beta$.

unit sphere representations. The relatively low on/off contrast computed across the series, and observed experimentally for $[\mathbf{3}]^{2-/3-}$, is consistent with delocalization of charge across the $\{Mo_6O_{18}N\}$ cluster—one electron reduction results in an average oxidation state change of only −0.167 per Mo, and an increase in average d-orbital occupancy from 0 to 0.167, so that switch off of LPCT will be far from complete. Thus, it seems likely that the much larger contrast experimentally reported[11] for $[\mathbf{1s}]^{2-/3-}$ is partly a result of different resonance and absorption effects in the two states.

https://doi.org/10.1021/acs.inorgchem.5c00915
Inorg. Chem. 2025, 64, 8408−8420

CONCLUSIONS

A family of new, sterically protected POM-based charge transfer chromophores with diphenylacetylene bridges has been synthesized. All four new compounds show high second-order nonlinear optical activity, without long wavelength absorption (λ_{max} < 450 nm in all cases), and using a julolidine donor system produced the highest $\beta_{0,zzz}$ yet reported for this class of compounds, with only a small red shift compared to the next highest performing. Moreover, extending the study to include a 2-dimensional (V-shaped) CT system based on a C_{2v} *bis*-donor POM indicates that such derivatives can have higher NLO activity than 1-D dipolar analogues, with no red shift in absorption profile. Redox-switched HRS experiments on the julolidinyl derivatized compound demonstrated reversible responses from a higher starting activity than seen previously; however, contrast was less than previously reported for an $-NMe_2$ donor system with a phenyl bridge. Nonetheless, TD-DFT calculations suggest that extended conjugated systems may increase on/off contrast and indicate that experimentally observed contrast may be strongly affected by resonance effects. The reduced states of the extended species studied were not sufficient for multicycle switching in solution, likely due to a decomposition mechanism that results in production of $[Mo_2O_7]^{2-}$ and appears to be favored by extended arylimido ligands. Consequently, while steric bulk around the imido-group clearly stabilizes arylimido-polyoxometalate-reduced states, switched second-order NLO contrast and multicycle stability appear to vary quite strongly with the imido-aryl ligand. Work to better understand this, mitigate decomposition processes, and extend our study to more multidimensional POM-based chromophores is ongoing.

ASSOCIATED CONTENT

Data Availability Statement

In addition to the supporting information and deposited cif files, data can be obtained by contacting the corresponding author and will be deposited at DOI: 10.17635/Lancaster/researchdata/705.

Supporting Information

The Supporting Information is available free of charge at https://pubs.acs.org/doi/10.1021/acs.inorgchem.5c00915.

Full synthetic details for organic precursor compounds, including characterization, X-ray crystallographic details including tabulated bond lengths, cyclic voltammograms, full computational details including calculated bond lengths, UV−vis spectra, and CT descriptors (PDF)

Cartesian coordinates of computed geometries (ZIP)

Accession Codes

Deposition Numbers 2425862−2425866 contain the supplementary crystallographic data for this paper. These data can be obtained free of charge via the joint Cambridge Crystallographic Data Centre (CCDC) and Fachinformationszentrum Karlsruhe Access Structures service.

AUTHOR INFORMATION

Corresponding Authors

Benoît Champagne − *Unit of Theoretical and Structural Physical Chemistry, Namur Institute of Structured Matter, University of Namur, Namur B-5000, Belgium;* orcid.org/0000-0003-3678-8875; Email: Benoit.Champagne@unamur.be

Koen Clays − *Department of Chemistry, University of Leuven, Leuven 3001, Belgium*; Email: Koen.Clays@kuleuven.be

John Fielden − *Department of Chemistry, Lancaster University, Lancaster LA1 4YW, U.K.; School of Chemistry, University of East Anglia, Norwich NR4 7TJ, U.K.;* orcid.org/0000-0001-5963-7792; Email: j.fielden@lancaster.ac.uk

Authors

Bethany R. Hood − *Department of Chemistry, Lancaster University, Lancaster LA1 4YW, U.K.; School of Chemistry, University of East Anglia, Norwich NR4 7TJ, U.K.*

Yovan de Coene − *Department of Chemistry, University of Leuven, Leuven 3001, Belgium;* orcid.org/0000-0002-1514-5865

Claire F. Jones − *School of Chemistry, Pharmacy and Pharmacology, University of East Anglia, Norwich NR4 7TJ, U.K.*

Noah Deveaux − *Unit of Theoretical and Structural Physical Chemistry, Namur Institute of Structured Matter, University of Namur, Namur B-5000, Belgium;* orcid.org/0009-0004-2945-6383

Jack M. Barber − *School of Chemistry, University of East Anglia, Norwich NR4 7TJ, U.K.*

Charlotte G. Marshall − *School of Chemistry, University of East Anglia, Norwich NR4 7TJ, U.K.*

Chloe A. Jordan − *School of Chemistry, University of East Anglia, Norwich NR4 7TJ, U.K.*

Nathan R. Halcovitch − *Department of Chemistry, Lancaster University, Lancaster LA1 4YW, U.K.;* orcid.org/0000-0001-6831-9681

Complete contact information is available at: https://pubs.acs.org/10.1021/acs.inorgchem.5c00915

Author Contributions

The manuscript was written through contributions of all authors. All authors have given approval to the final version of the manuscript.

Notes

The authors declare no competing financial interest.

ACKNOWLEDGMENTS

We thank the EPSRC for support through grant EP/M00452X/1 to J.F.. X-ray data were obtained in facilities established by EPSRC grant EP/S005854/1. B.R.H. thanks the University of East Anglia for a studentship and Lancaster University for short-term postdoctoral support. C.F.J. and J.F. acknowledge funding from the Leverhulme Trust (RPG-2020-365). Y.D.C. acknowledges the Fonds Wetenschappelijk Onderzoek (FWO) for senior postdoc (No. 1268825N). N.D. thanks the F.R.S-FNRS and the Walloon Region for his FRIA grant. Calculations were performed on the Consortium des Équipements de Calcul Intensif (CECI, http://www.ceci-hpc.be) and the Technological Platform of High-Performance Computing, for which the authors acknowledge the financial support of the FNRS-FRFC, the Walloon Region, and University of Namur (Convention Nos. GEQ U.G006.15, U.G018.19, U.G011.22, RW1610468, RW/GEQ2016, RW1117545, and RW2110213).

ABBREVIATION

POM, polyoxometalate

https://doi.org/10.1021/acs.inorgchem.5c00915
Inorg. Chem. 2025, 64, 8408−8420

REFERENCES

(1) (a) *Polyoxometalates: from Platonic Solids to Anti-Retroviral Activity*; Pope, M. T., Müller, A., Eds.; Kluwer Academic Publishers: Dordrecht, The Netherlands, 1994. (b) Miras, H. N.; Yan, J.; Long, D.-L.; Cronin, L. Engineering Polyoxometalates with Emergent Properties. *Chem. Soc. Rev.* **2012**, *41*, 7403−7430.

(2) (a) Müller, A.; Krickenmeyer, E.; Bögge, H.; Schmidtmann, M.; Peters, F. Organizational Forms of Matter: An Inorganic Super Fullerene and Keplerate Based on Molybdenum Oxide. *Angew. Chem., Int. Ed.* **1998**, *37*, 3359−3363. (b) Müller, A.; Beckmann, E.; Bögge, H.; Schmidtmann, M.; Dress, A. Inorganic Chemistry Goes Protein Size: A Mo_{368} Nano-Hedgehog Initiating Nanochemistry by Symmetry Breaking. *Angew. Chem., Int. Ed.* **2002**, *41*, 1162−1167.

(3) (a) Neumann, R.; Dahan, M. A Ruthenium-Substituted Polyoxometalate as an Inorganic Dioxygenase for Activation of Molecular Oxygen. *Nature* **1997**, *388*, 353−355. (b) Sumliner, J. M.; Lv, H.; Fielden, J.; Geletii, Y. V.; Hill, C. L. Polyoxometalate Multi-Electron-Transfer Catalytic Systems for Water Splitting. *Eur. J. Inorg. Chem.* **2014**, *2014*, 635−644. (c) Lv, H.; Guo, W.; Wu, K.; Chen, Z.; Bacsa, J.; Musaev, D. G.; Geletii, Y. V.; Lauinger, S. M.; Lian, T.; Hill, C. L. A Noble-Metal-Free, Tetra-Nickel Polyoxotungstate Catalyst for Efficient Photocatalytic Hydrogen Evolution. *J. Am. Chem. Soc.* **2014**, *136*, 14015−14018. (d) Haider, A.; Bassil, B. S.; Soriano-López, J.; Qasim, H. M.; Sáenz de Pipaón, C.; Ibrahim, M.; Dutta, D.; Koo, Y.-S.; Carbó, J. J.; Poblet, J. M.; Galán-Mascaros, J. R.; Kortz, U. 9-Cobalt(II)-Containing 27-Tunsgsto-3-Germanate(IV): Synthesis, Structure, Computational Modeling and Heterogeneous Water Oxidation Catalysis. *Inorg. Chem.* **2019**, *58*, 11308−11316.

(4) (a) Bijelic, M.; Aureliano, A.; Rompel, A. Polyoxometalates as Potential Next-Generation Metallodrugs in the Combat Against Cancer. *Angew. Chem., Int. Ed.* **2019**, *58*, 2980−2999. (b) She, S.; Bian, S.; Huo, R.; Chen, K.; Huang, Z.; Zhang, J.; Hao, J.; Wei, Y. Degradable Organically-Derivatized Polyoxometalate with Enhanced Activity against Glioblastoma Cell Line. *Sci. Rep.* **2016**, *6*, 33529.

(5) (a) Busche, C.; Vilà-Nadal, L.; Yan, J.; Miras, H. N.; Long, D.-L.; Georgiev, V. P.; Asenov, A.; Pedersen, R. H.; Gadegaard, N.; Mirza, M. M.; Paul, D. J.; Poblet, J. M.; Cronin, L. Design and Fabrication of Memory Devices based on Nanoscale Polyoxometalate Clusters. *Nature* **2014**, *515*, 545−549. (b) Linnenberg, O.; Moors, M.; Notario-Estévez, A.; López, X.; de Graaf, C.; Peter, S.; Baeumer, C.; Waser, R.; Monakhov, K. Y. Adressing Multiple Resistive States of Polyoxovanadates: Conductivity as a Function of Individual Molecular Redox States. *J. Am. Chem. Soc.* **2018**, *140*, 16635−16640. (c) Huez, C.; Guérin, D.; Lenfant, S.; Volatron, F.; Calame, M.; Perrin, M.; Proust, A.; Vuillaume, D. Redox-Controlled Conductance of Polyoxometalate Molecular Junctions. *Nanoscale* **2022**, *14*, 13790−13800. (d) Chen, X.; Huang, P.; Zhu, X.; Zhuang, S.; Zhu, H.; Fu, J.; Nissimagoudar, A. S.; Li, W.; Zhang, X.; Zhou, L.; Wang, Y.; Lv, Z.; Zhou, Y.; Han, S.-T. Keggin-Type Polyoxometalate Cluster as an Active Component for Redox-Based Nonvolatile Memory. *Nanoscale Horiz.* **2019**, *4*, 697−704.

(6) (a) Dolbecq, A.; Dumas, E.; Mayer, C. R.; Mialane, P. Hybrid Organic−Inorganic Polyoxometalate Compounds: From Structural Diversity to Applications. *Chem. Rev.* **2010**, *110*, 6009−6048. (b) Proust, A.; Matt, B.; Villanneau, R.; Guillemot, G.; Gouzerh, P.; Izzet, G. Functionalization and Post-Functionalization: A Step Towards Polyoxometalate-Based Materials. *Chem. Soc. Rev.* **2012**, *41*, 7605−7622. (c) Zhang, J.; Xiao, F.; Hao, J.; Wei, Y. The Chemistry of Organoimido Derivatives of Polyoxometalates. *Dalton Trans.* **2012**, *41*, 3599−3615. (d) Pardiwala, A.; Kumar, S.; Jangir, R. Insights into Organic-Inorganic Hybrid Molecular Materials: Organoimido Functionalized Polyoxometalates. *Dalton Trans.* **2022**, *51*, 4945−4975. (e) Cameron, J. M.; Guillemot, G.; Galambos, T.; Amin, S. S.; Hampson, E.; Mall Haidaraly, K.; Newton, G. N.; Izzet, G. Supramolecular Assemblies of Organo-Functionalised Hybrid Polyoxometalates: From Functional Building Blocks to Hierarchical Nanomaterials. *Chem. Soc. Rev.* **2022**, *51*, 293−328.

(7) (a) Al-Yasari, A.; Van Steerteghem, N.; El Moll, H.; Clays, K.; Fielden, J. Donor−Acceptor Organo-Imido Polyoxometalates: High Transparency, High Activity Redox-Active NLO Chromophores. *Dalton Trans.* **2016**, *45*, 2818−2822. (b) Al-Yasari, A.; Van Steerteghem, N.; Kearns, H.; El Moll, H.; Faulds, K.; Wright, J. A.; Brunschwig, B. S.; Clays, K.; Fielden, J. Organoimido-Polyoxometalate Nonlinear Optical Chromophores: A Structural, Spectroscopic, and Computational Study. *Inorg. Chem.* **2017**, *56*, 10181−10194. (c) Al-Yasari, A.; Spence, P.; El Moll, H.; Van Steerteghem, N.; Horton, P. N.; Brunschwig, B. S.; Clays, K.; Fielden, J. Fine-Tuning Polyoxometalate Non-Linear Optical Chromophores: A Molecular Electronic "Goldilocks" Effect. *Dalton Trans.* **2018**, *47*, 10415−10419. (d) Jones, C. F.; Hood, B. R.; de Coene, Y.; Lopez-Poves, I.; Champagne, B.; Clays, K.; Fielden, J. Bridge Improvement Work: Maximising Non-Linear Optical Performance in Polyoxometalate Derivatives. *Chem. Commun.* **2024**, *60*, 1731−1734. (e) Rtibi, E.; Abderrabba, M.; Ayadi, S.; Champagne, B. Theoretical Assessment of the Second-Order Nonlinear Optical Responses of Lindqvist-Type Organoimido Polyoxometalates. *Inorg. Chem.* **2019**, *58*, 11210−11219. (f) Al-Yasari, A.; El Moll, H.; Purdy, R.; Vincent, K. B.; Spence, P.; Malval, J.-P.; Fielden, J. Optical, Third Order Non-Linear Optical and Electrochemical Properties of Dipolar, Centrosymmetric and C_{2v} Organoimido Polyoxometalate Derivatives. *Phys. Chem. Chem. Phys.* **2021**, *23*, 11807−11817.

(8) (a) *Nonlinear Optics of Organic Molecules and Polymers*; Nalwa, H. S., Miyata, S., Eds.; CRC Press: Boca Raton, FL, 1997. (b) Marder, S. R. Organic Nonlinear Optical Materials: Where We Have Been and Where We Are Going. *Chem. Commun.* **2006**, 131−134. (c) Kuzyk, M. G. Using Fundamental Principles to Understand and Optimize Nonlinear-Optical Materials. *J. Mater. Chem.* **2009**, *19*, 7444−7465.

(9) (a) Kang, H.; Facchetti, A.; Jiang, H.; Cariati, E.; Righetto, S.; Ugo, R.; Zuccaccia, C.; Macchioni, A.; Stern, C. L.; Liu, Z.; Ho, S. T.; Brown, E. C.; Ratner, M. A.; Marks, T. J. Ultralarge Hyperpolarizability Twisted π-Electron System Electro-Optic Chromophores: Synthesis, Solid-State and Solution-Phase Structural Characteristics, Electronic Structures, Linear and Nonlinear Optical Properties, and Computational Studies. *J. Am. Chem. Soc.* **2007**, *129*, 3267. (b) Shi, Y.; Frattarelli, D.; Watanabe, N.; Facchetti, A.; Cariati, E.; Righetto, S.; Tordin, E.; Zuccaccia, C.; Macchioni, A.; Wegener, S. L.; Stern, C. L.; Ratner, M. A.; Marks, T. J. Ultra-High-Response, Multiply Twisted Electro-Optic Chromophores: Influence of π-System Elongation and Interplanar Torsion on Hyperpolarizability. *J. Am. Chem. Soc.* **2015**, *137*, 12521. (c) Beverina, L.; Sanguineti, A.; Battagliarin, G.; Ruffo, R.; Roberto, D.; Righetto, S.; Soave, R.; Lo Presti, L.; Ugo, R.; Pagani, G. A. UV Absorbing Zwitterionic Pyridinium-Tetrazolate: Exceptional Transparency/Optical Nonlinearity Trade-Off. *Chem. Commun.* **2011**, *47*, 292−294.

(10) (a) Coe, B. J.; Houbrechts, S.; Asselberghs, I.; Persoons, A. Efficient, Reversible Redox-Switching of Molecular First Hyperpolarizabilities in Ruthenium(II) Complexes Possessing Large Quadratic Optical Nonlinearities. *Angew. Chem., Int. Ed.* **1999**, *38*, 366−369. (b) Sporer, C.; Ratera, I.; Ruiz-Molina, D.; Zhao, Y.; Vidal-Gancedo, J.; Wurst, K.; Jaitner, P.; Clays, K.; Persoons, A.; Rovira, C.; Veciana, J. A Molecular Multiproperty Switching Array Based on the Redox Behavior of a Ferrocenyl Polychlorotriphenylmethyl Radical. *Angew. Chem., Int. Ed.* **2004**, *43*, 5266−5268. (c) Boubekeur-Lecaque, L.; Coe, B. J.; Clays, K.; Foerier, S.; Verbiest, T.; Asselberghs, I. Redox-Switching of Nonlinear Optical Behavior in Langmuir−Blodgett Thin Films Containing a Ruthenium(II) Ammine Complex. *J. Am. Chem. Soc.* **2008**, *130*, 3286−3287. (d) Boixel, J.; Guerchais, V.; Le Bozec, H.; Jacquemin, D.; Amar, A.; Boucekkine, A.; Colombo, A.; Dragonetti, C.; Marinotto, D.; Roberto, D.; Righetto, S.; De Angelis, R. Second-Order NLO Switches from Molecules to Polymer Films Based on Photochromic Cyclometalated Platinum(II) Complexes. *J. Am. Chem. Soc.* **2014**, *136*, 5367−5375. (e) Beaujean, P.; Bondu, F.; Plaquet, A.; Garcia-Amorós, J.; Cusido, J.; Raymo, F. M.; Castet, F.; Rodriguez, V.; Champagne, B. Oxazines: A New Class of Second-Order Nonlinear Optical Switches. *J. Am. Chem. Soc.* **2016**, *138*, 5052−5062.

(11) Hood, B. R.; de Coene, Y.; Torre Do Vale Froes, A. V.; Jones, C. F.; Beaujean, P.; Liégeois, V.; MacMillan, F.; Champagne, B.;

https://doi.org/10.1021/acs.inorgchem.5c00915
Inorg. Chem. 2025, 64, 8408−8420

Clays, K.; Fielden, J. Electrochemically-Switched 2nd Order Non-Linear Optical Response in an Arylimido-Polyoxometalate with High Contrast and Cyclability. *Angew. Chem., Int. Ed.* **2023**, *62*, No. e202215537.
(12) Klemperer, W. G. Tetrabutylammonium Isopolyoxometalates. *Inorg. Synth.* **1990**, *27*, 74−85.
(13) Ibrahim, S. K.. Ph.D. Thesis, University of Sussex, 1992.
(14) Krejčik, M.; Daněk, M.; Hartl, F. Simple Construction of an Infrared Optically Transparent Thin-Layer Electrochemical Cell: Applications to the Redox Reactions of Ferrocene, $Mn_2(CO)_{10}$ and $Mn(CO)_3$(3,5-di-t-Butyl-catecholate)$^-$. *J. Electroanal. Chem.* **1991**, *317*, 179−187.
(15) *CrysAlisPro*, (Version 1.171.40.68a); Rigaku Oxford Diffraction, Rigaku Corporation: Tokyo, Japan, 2019.
(16) Sheldrick, G. M. SHELXT—Integrated Space-Group and Crystal-Structure Determination. *Acta Crystallogr., Sect. A: Found. Adv.* **2015**, *71*, 3−8.
(17) Dolomanov, O. V.; Bourhis, L. J.; Gildea, R. J.; Howard, J. A. K.; Puschmann, H. OLEX2: A Complete Structure Solution, Refinement and Analysis Program. *J. Appl. Crystallogr.* **2009**, *42*, 339−341.
(18) Sheldrick, G. M. Crystal Structure Refinement with SHELXL. *Acta Crystallogr., Sect. C: Struct. Chem.* **2015**, *71*, 3−8.
(19) (a) Clays, K.; Persoons, A. Hyper-Rayleigh Scattering in Solution. *Phys. Rev. Lett.* **1991**, *66*, 2980−2983. (b) Clays, K.; Persoons, A. Hyper-Rayleigh Scattering in Solution. *Rev. Sci. Instrum.* **1992**, *63*, 3285−3289. (c) Hendrickx, E.; Clays, K.; Persoons, A. Hyper-Rayleigh Scattering in Isotropic Solution. *Acc. Chem. Res.* **1998**, *31*, 675−683.
(20) (a) Olbrechts, G.; Strobbe, R.; Clays, K.; Persoons, A. High-Frequency Demodulation of Multi-Photon Fluorescence in Hyper-Rayleigh Scattering. *Rev. Sci. Instrum.* **1998**, *69*, 2233−2241. (b) Olbrechts, G.; Wostyn, K.; Clays, K.; Persoons, A. High-Frequency Demodulation of Multiphoton Fluorescence in Long-Wavelength hyper-Rayleigh Scattering. *Opt. Lett.* **1999**, *24*, 403−405. (c) Clays, K.; Wostyn, K.; Olbrechts, G.; Persoons, A.; Watanabe, A.; Nogi, K.; Duan, X.-M.; Okada, S.; Oikawa, H.; Nakanishi, H.; Vogel, H.; Beljonne, D.; Brédas, J.-L. Fourier Analysis of the Femtosecond Hyper-Rayleigh Scattering Signal from Ionic Fluorescent Hemicyanine Dyes. *J. Opt. Soc. Am. B* **2000**, *17*, 256−265. (d) Franz, E.; Harper, E. C.; Coe, B. J.; Zahradnik, P.; Clays, K.; Asselberghs, I. Benzathiazoliums and Pyridiniums for Second-Order Nonlinear Optics. *Organic Optoelectronics and Photonics III, Proc. SPIE*, 2008, Vol. *6999*, p. 699923..
(21) Campo, J.; Desmet, F.; Wenseleers, W.; Goovaerts, E. Highly Sensitive Setup for Tunable Wavelength Hyper-Rayleigh Scattering with Parallel Detection and Calibration Data for Various Solvents. *Opt. Express* **2009**, *17*, 4587−4604.
(22) (a) Heesink, G. J. T.; Ruiter, A. G. T.; van Hulst, N. F.; Bölger, B. Determination of Hyperpolarizability Tensor Components by Depolarized Hyper-Rayleigh Scattering. *Phys. Rev. Lett.* **1993**, *71*, 999−1002. (b) Hendrickx, E.; Boutton, C.; Clays, K.; Perssons, A.; van Es, S.; Biemans, T.; Meijer, B. Quadratic Nonlinear Optical Properties of Correlated Chromophores: Cyclic 6,6′-Dinitro-1,1′-binaphthyl-2,2′-ethers. *Chem. Phys. Lett.* **1997**, *270*, 241−244. (c) Boutton, C.; Clays, K.; Persoons, A.; Wada, T.; Sasabe, H. Second-Order Off-Diagonal Hyperpolarizability Tensor Components of Substituted Carbazoles by Hyper-Rayleigh Scattering Depolarization Measurements. *Chem. Phys. Lett.* **1998**, *286*, 101−106. (d) Castet, F.; Bogdan, E.; Plaquet, A.; Ducasse, L.; Champagne, B.; Rodriguez, V. Reference Molecules for Nonlinear Optics: A Joint Experimental and Theoretical Investigation. *J. Chem. Phys.* **2012**, *136*, 024506.
(23) Chai, J. D.; Head-Gordon, M. Long-Range Corrected Hybrid Density Functionals with Damped Atom-Atom Dispersion Corrections. *Phys. Chem. Chem. Phys.* **2008**, *10*, 6615−6620.
(24) Krishnan, R.; Binkley, J. S.; Seeger, R.; Pople, J. A. Self-Consistent Molecular Orbital Methods. XX. A Basis Set for Correlated Wavefunctions. *J. Chem. Phys.* **1980**, *72*, 650−654.
(25) Roy, L. E.; Hay, P. J.; Martin, R. L. Revised Basis Sets for the LANL Effective Core Potentials. *J. Chem. Theory Comput.* **2008**, *4*, 1029−1031.
(26) Tomasi, J.; Mennucci, B.; Cammi, R. Quantum Mechanical Continuum Solvation Models. *Chem. Rev.* **2005**, *105*, 2999−3094.
(27) Casida, M. E.. In *Recent Advances in Density Functional Theory*; Chong, D. P., Ed.; World Scientific: Singapore, 1995; pp 155−192.
(28) Le Bahers, T.; Adamo, C.; Ciofini, I. A. Qualitative Index of Spatial Extent in Charge-Transfer Excitations. *J. Chem. Theory Comput.* **2011**, *7*, 2498−2506.
(29) (a) Van Gisbergen, S. J. A.; Snijders, J. G.; Baerends, E. J. Calculating Frequency-Dependent Hyperpolarizabilities using Time-Dependent Density Functional Theory. *J. Chem. Phys.* **1998**, *109*, 10644−10656. (b) Helgaker, T.; Coriani, S.; Jørgensen, P.; Kristensen, K.; Olsen, J.; Ruud, K. Recent Advances in Wave Function-Based Methods of Molecular Property Calculautions. *Chem. Rev.* **2012**, *112*, 543−631.
(30) (a) de Wergifosse, M.; Champagne, B. Electron Correlation Effects on the First Hyperpolarizability of Push-Pull π-Conjugated Systems. *J. Chem. Phys.* **2011**, *134*, 074113. (b) Johnson, L. E.; Dalton, L. R.; Robinson, B. H. Optimising Calculations of Electronic Excitations and Relative Hyperpolarizabilities of Electrooptic Chromophores. *Acc. Chem. Res.* **2014**, *47*, 3258−3265. (c) Garrett, K.; Sosa Vazquez, X. A.; Egri, S. B.; Wilmer, J.; Johnson, L. E.; Robinson, B. H.; Isborn, C. M. Optimum Exchange for Calculation of Excitation Energies and Hyperpolarizabilities of Organic Electro-Optic Chromophores. *J. Chem. Theory Comput.* **2014**, *10*, 3821−3831.
(31) Coe, B. J.; Fielden, J.; Foxon, S. P.; Harris, J. A.; Helliwell, M.; Brunschwig, B. S.; Asselberghs, I.; Clays, K.; Garín, J.; Orduna, J. Diquat Derivatives: Highly Active, Two-Dimensional Nonlinear Optical Chromophores with Potential Redox Switchability. *J. Am. Chem. Soc.* **2010**, *132*, 10498−10512.
(32) (a) Wei, Y.; Xu, B.; Barnes, C. L.; Peng, Z. An Efficient and Convenient Reaction Protocol to Organoimido Derivatives of Polyoxometalates. *J. Am. Chem. Soc.* **2001**, *123*, 4083−4084. (b) Bar-Nahum, I.; Narasimhulu, K. V.; Weiner, L.; Neumann, R. Phenanthroline−Polyoxometalate Hybrid Compounds and the Observation of Intramolecular Charge Transfer. *Inorg. Chem.* **2005**, *44*, 4900−4902.
(33) Xu, L.; Lu, M.; Xu, B.; Wei, Y.; Peng, Z.; Powell, D. R. Towards Main-Chain-Polyoxometalate-Containing Hybrid Polymers: A Highly Efficient Approach to Bifunctionalized Organoimido Derivatives of Hexamolybdates. *Angew. Chem., Int. Ed.* **2002**, *41*, 4129−4132.
(34) (a) Xia, Y.; Wei, Y.; Wang, Y.; Guo, H. A Kinetically Controlled Trans Bifunctionalized Organoimido Derivative of the Lindqvist-Type Hexamolybdate: Synthesis, Spectroscopic Characterization, and Crystal Structure of $(n\text{-}Bu_4N)_2\{trans\text{-}[Mo_6O_{17}(NAr)_2]$. *Inorg. Chem.* **2005**, *44*, 9823−9828. (b) Qin, C.; Wang, X.; Xu, L.; Wei, Y. A Linear Bifunctionalized Organoimido Derivative of Hexamolybdate: Convenient Synthesis and Crystal Structure. *Inorg. Chem. Commun.* **2005**, *8*, 751−754.
(35) (a) Lin, V. S.; Therien, M. J. The Role of Porphyrin-to-Porphyrin Linkage Topology in the Extensive Modulation of the Absorptive and Emissive Properties of a Series of Ethynyl- and Butadiynyl-Bridged Bis- and Tris(porphinato)zinc Chromophores. *Chem.—Eur. J.* **1995**, *1* (9), 645−651. (b) LeCours, S. M.; DiMagno, S. G.; Therien, M. J. Exceptional Electronic Modulation of Porphyrins through meso-Arylethynyl Groups. Electronic Spectroscopy, Electronic Structure, and Electrochemistry of [5,15-Bis[(aryl)ethynyl]-10,20-diphenylporphinato]zinc(II) Complexes. X-ray Crystal Structures of [5,15-Bis[(4′-fluorophenyl)ethynyl]-10,20-diphenylporphinato]zinc(II) and 5,15-Bis[(4′-methoxyphenyl)-ethynyl]-10,20-diphenylporphyrin. *J. Am. Chem. Soc.* **1996**, *118*, 11854−11864. (c) Kamat, N. P.; Liao, Z.; Moses, L. E.; Rawson, J.; Therien, M. J.; Dmochowski, I. J.; Hammer, D. A. Sensing Membrane Stress with Near IR-Emissive Porphyrins. *Proc. Natl. Acad. Sci. U.S.A.* **2011**, *108*, 13984−13989.

https://doi.org/10.1021/acs.inorgchem.5c00915
Inorg. Chem. 2025, 64, 8408−8420

(36) Al-Yasari, A. Synthesis, Non-Linear Optical and Electrochemical Properties of Novel Organoimido Polyoxometalate Derivatives. Ph.D. Thesis, University of East Anglia, 2016.
(37) Weinstock, I. A. Homogeneous-Phase Electron-Transfer Reactions of Polyoxometalates. *Chem. Rev.* **1998**, *98*, 113−170.
(38) Cao, J.; Wang, Q.; Liu, C.; An, S. Gas-Phase Chemistry of Arylimido-Functionalized Hexamolybdates $[Mo_6O_{19}]^{2-}$. *J. Am. Soc. Mass Spectrom.* **2018**, *29*, 1331−1334.
(39) (a) Oudar, J. L.; Chemla, D. S. Hyperpolarizabilities of the Nitroanilines and their Relations to the Excited State Dipole Moment. *J. Chem. Phys.* **1977**, *66*, 2664−2668. (b) Oudar, J. L. Optical Nonlinearities of Conjugated Molecules. Stilbene Derivatives and Highly Polar Aromatic Compounds. *J. Chem. Phys.* **1977**, *67*, 446−457.
(40) Che, M.; Fournier, M.; Launay, J. P. The Analog of Surface Molybdenyl Ion in Mo/SiO_2 supported catalysts: the Isopolyanion $Mo_6O_{19}^{3-}$ Studied by EPR and UV-Visible Spectroscopy. Comparison with Other Molybdenyl Compounds. *J. Chem. Phys.* **1979**, *71*, 1954−1960.

https://doi.org/10.1021/acs.inorgchem.5c00915
Inorg. Chem. 2025, 64, 8408−8420